Institute of Aviation

Review of Polish Aeronautical
Fatigue Work 2005 – 2007

Antoni Niepokólczycki
May 2007

Warsaw, POLAND

CONTENTS

1. INTRODUCTION

This review gives a summary of work performed in Poland in the area of aeronautical fatigue during the period from April 2005 to March 2007.

The various contributions to this review come from the following sources:
Institute of Aviation, Warsaw;
Air Force Institute of Technology, Warsaw;
University of Mining and Metallurgy, Cracow;
Military University of Technology, Warsaw;
Rzeszow University of Technology, Rzeszow;
Warsaw University of Technology, Warsaw;
PZL ŚWIDNIK, Świdnik;
PZL MIELEC, Mielec.

The names of the principal investigators and their affiliations are presented between brackets at the end of each topic title.

Full addresses of contributors are available through the author of this review at:

Antoni NIEPOKÓLCZYCKI
Institute of Aviation
Al. Krakowska 110/114
02-256 Warsaw, POLAND
Phone: (+48-22) 846 08 01 ext. 546
Fax: (+48-22) 846 44 32
E-mail: antekn@ilot.edu.pl

2. HELICOPTERS

2.1 Fatigue Test of the PZL SW-4 Helicopter Rotor Head

(Marek Stawski – PZL ŚWIDNIK)

The rotor head of the PZL SW-4 helicopter was tested.

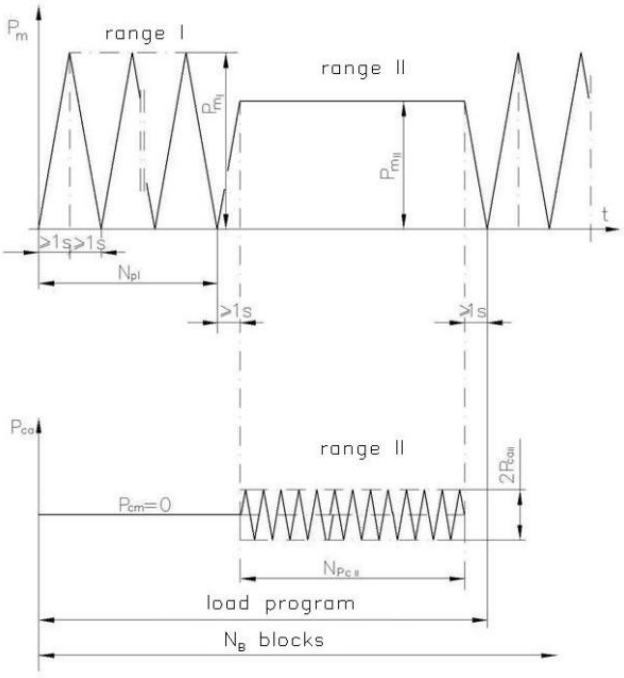

On the test stand a specimen was subjected to both the axial forces P_m applied to each arm of the hub and variable forces P_{ca} due to masses rotating at an angular velocity ω. In the thrust plane those forces generated a variable moment M_{ca}.
The magnitudes of P_{ca} resulted from a proper choice of the values of rotating masses and the angular velocity ω.

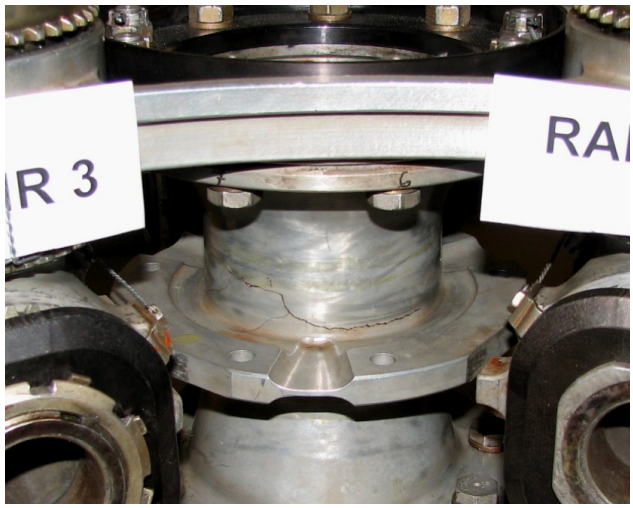

The testing was stopped after the application of 7909 loading blocks, when a crack was detected in the upper central part of the hub.

2.2 Full-scale Fatigue Tests of the Fin and Horizontal Stabilizer of PZL SW-4 Helicopter

(Marek Stawski – PZL ŚWIDNIK)

The fin as well as the horizontal stabilizer both with part of tail booms were subjected to tests. The investigations aimed at

- improving the fatigue life of the considered assemblies,
- finding critical elements of the assemblies in view of the fatigue strength.

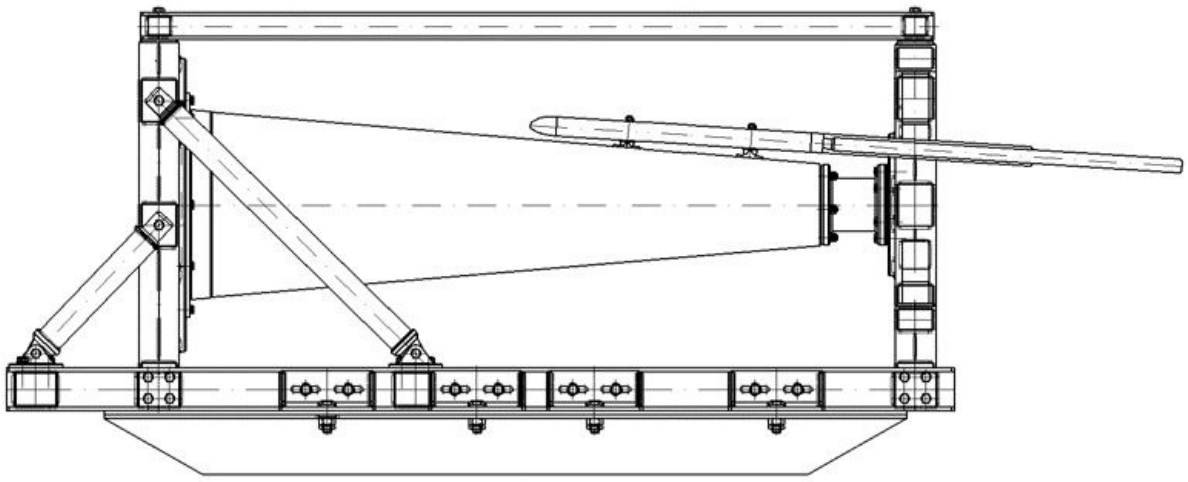

Fig. 2.2.1. Fin with a tail boom mounted on the test stand.

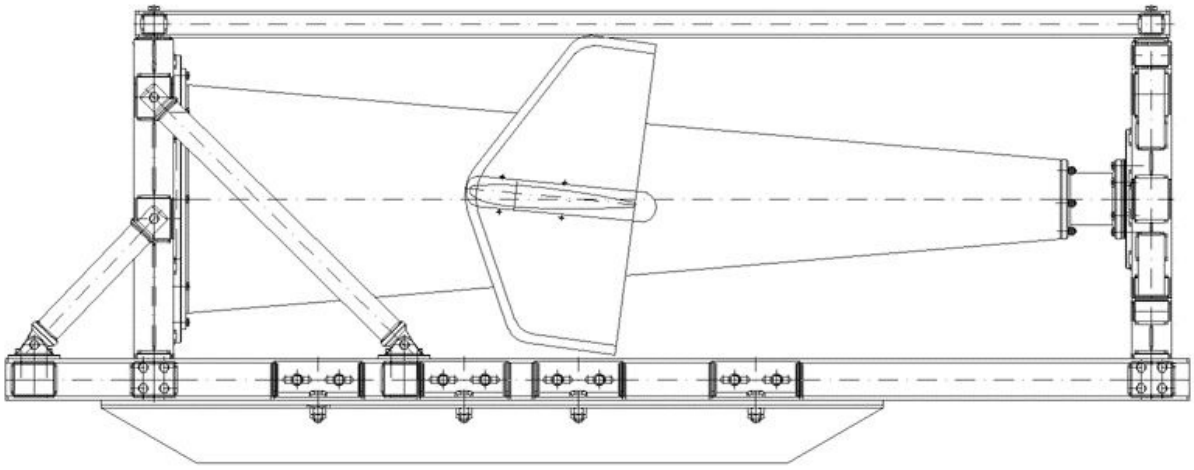

Fig. 2.2.2. Horizontal stabilizer with a tail boom mounted on the test stand.

A constant moment was applied to the fin. Variable loads were introduced by means of excitation of resonant vibrations of the fin on a vibrating table. The vibration frequency of 23.2 Hz has resulted from the vibration tests made before.
A constant moment was applied to the horizontal stabilizer. Variable loads also were introduced by means of excitation of resonant vibrations of the horizontal stabilizer on a vibrating table. The vibration frequency of 27.7 Hz has resulted from the vibration tests made before.
The test results were used in determination of the service lives of the considered assemblies.

2.3 Fatigue Test of the Tail Rotor Connector in the PZL SW-4 Helicopter

(Marek Stawski – PZL Świdnik)

The tail rotor connector of the SW-4 helicopter was subjected to fatigue testing at the PZL Świdnik. The test aimed at the fatigue life determination of a connector made from 17-7PH steel.

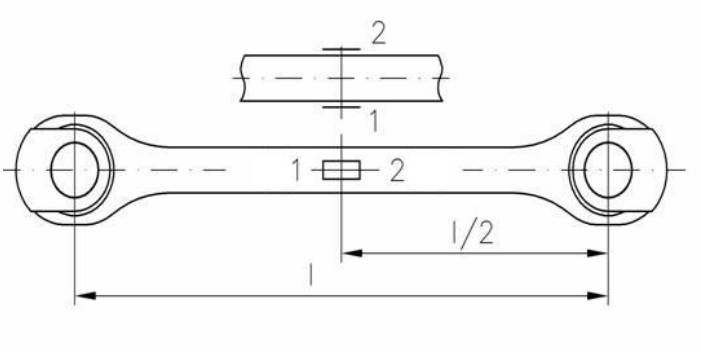

For each connector two strain gauges were used for measurement of the specimen loading.

Fig. 2.3.1.
Location of the strain gauges on the specimen.

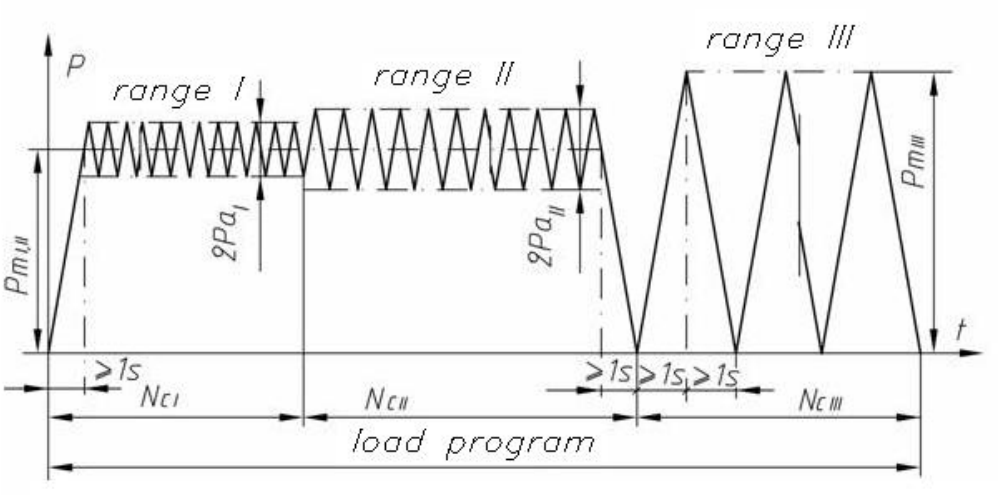

Test program

Range	Tensile force		No. of cycles in a block N_C	No. of blocks N_B
	Pm (const.)	Pa (var.)		
-	[daN]	[daN]	-	-
I	3687	270	5100	9000
II	3687	405	460	
III	4425	0	10	

First, the number of blocks was N_B = 9000, and then since the specimen did not fail, the loading was increased (by K = 1.5 in every range) and the new number of blocks was taken, i.e. N_{B2} = 1000.
Finally, the specimen failed after N_{B2} = 1043 of blocks.

2.4 Fatigue Test of a Helicopter Rotor Shaft

(Marek Stawski – PZL Świdnik)

The helicopter rotor shaft of W-3A helicopter was subjected to fatigue testing at the PZL Świdnik. The test aimed at the fatigue life determination of the shaft.

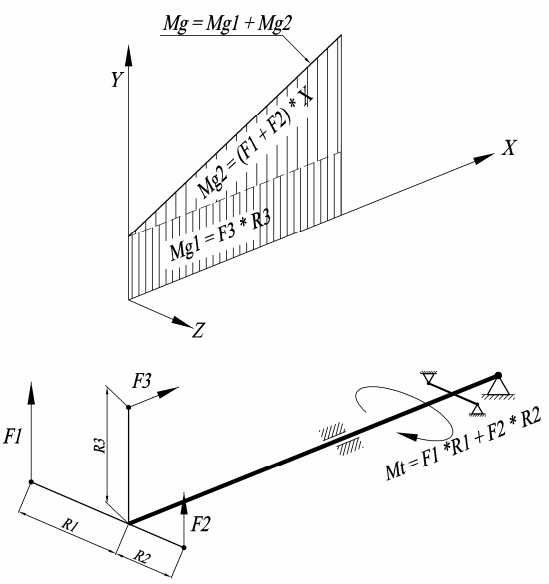

The tests were performer on the stand representing the conditions the shaft is subjected to in the helicopter (in view of geometry and kinematics).

Fig. 2.4.1. Loading scheme of the shaft.

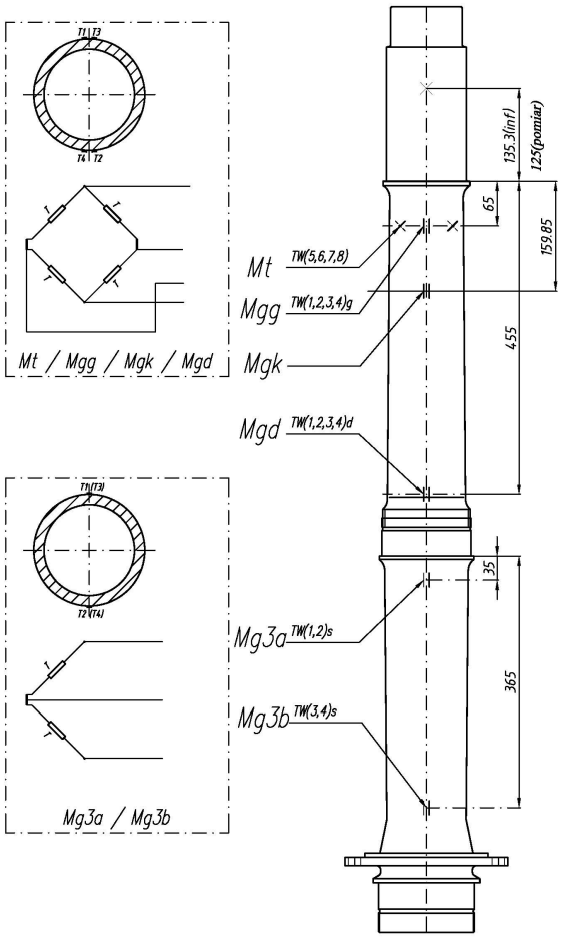

Fig. 2.4.2. Arrangement of strain gauges.

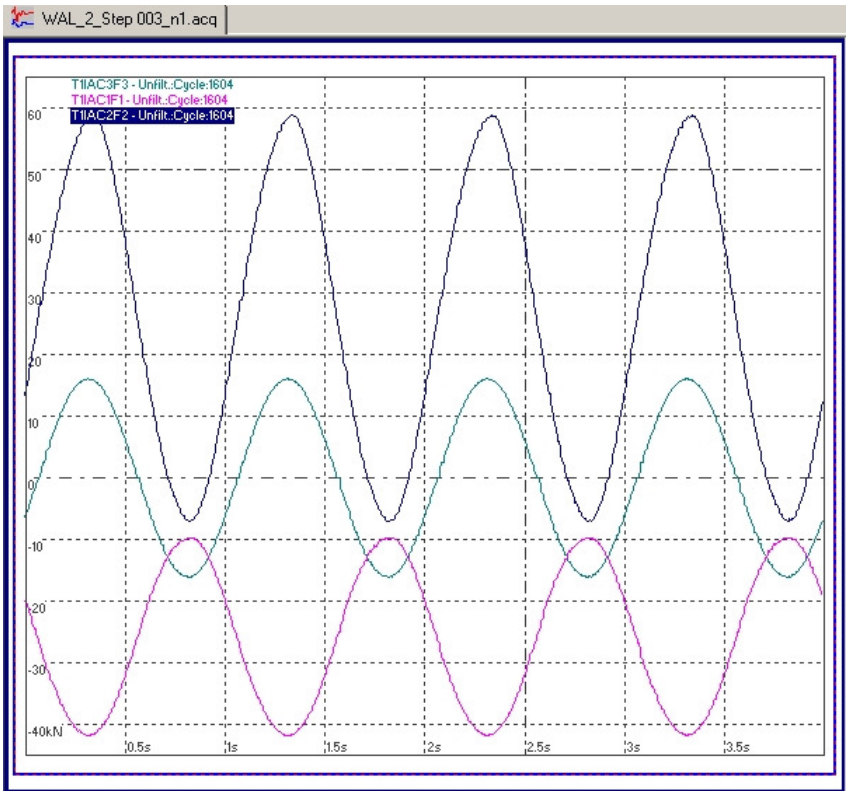

Fig. 2.4.3. Loading program.

The loading remained unchanged during the test. Both the investigated specimens failed after about 800 000 cycles.

2.5 Numerical Stress and Fatigue Analysis of the First Stage of a Helicopter Engine Turbine

(Lucjan Witek - Rzeszow University of Technology)

Researchers should solve a variety of problems when analyzing a high-speed turbine. One of them, the jet engine manufacturers have coped for decades, consists in failure due to the Low Cycle Fatigue, commonly referred to as LCF.
If a problem arises in the turbine section it will definitely affect the whole engine operation and, of course, the aircraft safety. The broken blade can stay within the engine cowl, while a disastrous failure of the turbine wheel can lead to a puncture of the engine cowl by larger segments of the disc. Failures of any high speed rotating components (jet engine rotors, high speed fans, etc.) can be very dangerous to passengers, personnel and on-board equipment, therefore should always be avoided by any means. In the present study, the attention is focused on a numerical analysis of stress and crack initiation at the first stage turbine components under the operational LCF conditions.

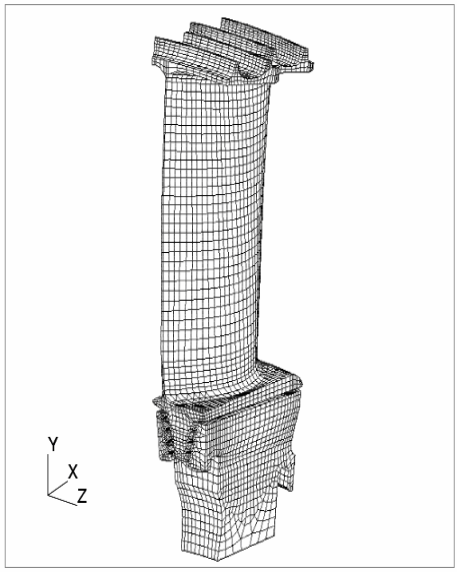

The stress analysis of turbine disc under the operational thermomechanical conditions was conducted. To this end, the finite element analysis of complex geometrical axisymmetrical model of turbine was carried out, the radial deformations resulting were then used to define boundary conditions for a 3D sub-model of the turbine segment consisting of one blade and part of disc (Fig. 2.5.1).

Fig. 2.5.1. Finite element model of the turbine segment.

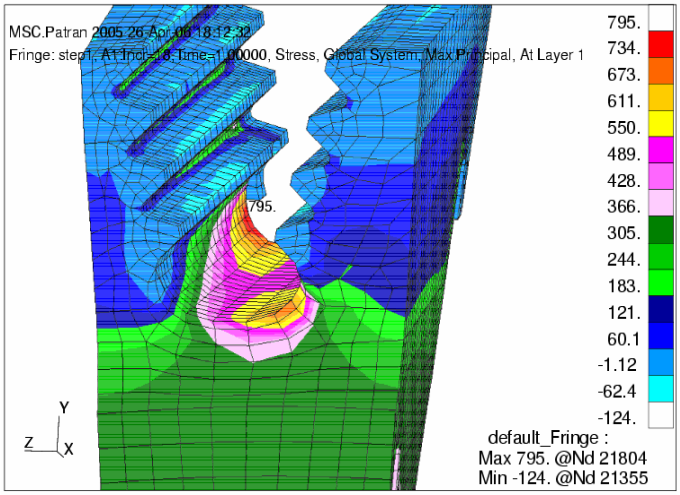

The stress contours resulted from a nonlinear static analysis performed for the turbine under operating conditions (Fig. 2.5.2). High stress zones were found at different regions of the turbine, where the initiation of fatigue cracks was expected. Critical nodes of the model (where the maximum stresses were observed) were then subjected to the fatigue analysis.

Fig. 2.5.2. Maximum stress (σ_1) distribution in the blade locking.

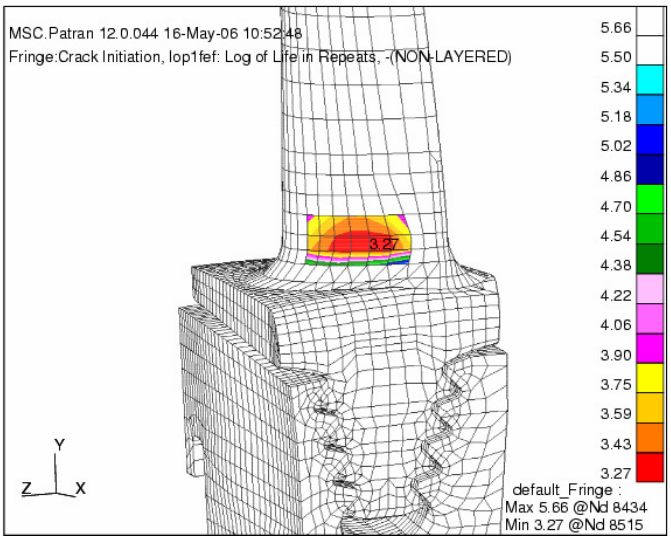

The results of numerical crack initiation (ε–N) analysis carried out for a simplified load history corresponding to 6-hour helicopter flight (basing on the laboratory long time fatigue test of engine) have been presented as well. The number hours of flight before the fatigue crack initiation in the critical components of turbine were estimated (Fig. 2.5.3).

Fig. 2.5.3. Results of ε-N analysis – number of hours to the crack initiation and location of the fatigue critical region for the blade. The time before the crack initiation in the blade is $10^{3,7032} \times 6 = 32376$ hours of engine operation.

The critical areas of turbine (in view of both the static and fatigue strength) are located on the blade lockings. In these regions both the maximum stress and the minimum fatigue life were observed (Fig. 2.5.2, Fig. 2.5.4). These zones should be subjected to a detailed visual inspection on a regular basis due to high probability of the fatigue crack initiation.

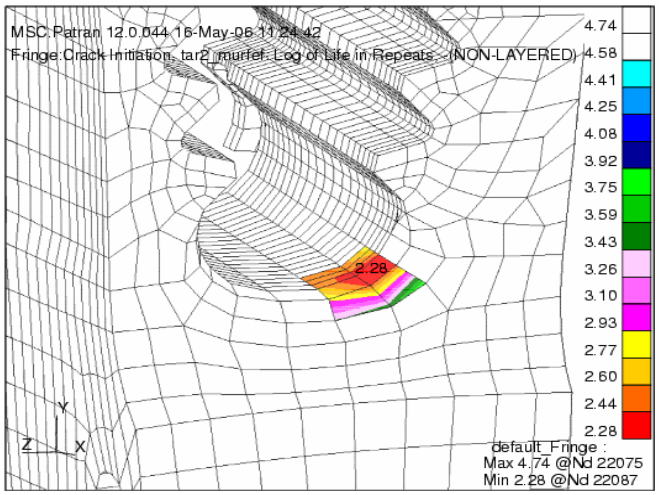

Fig. 2.5.4. Results of ε-N analysis for the bottom serration region of the turbine disc.

2.6 Application of Neural Networks to Determination of the Helicopter Rotor Loads

(Jarosław Stanisławski – Intitute of Aviation)

The magnitudes of load acting on a helicopter rotor depend mainly on flight parameters and the position of collective pitch control system and cyclic pitch control system.
Basing on easy available measurement results the application of neural network allows for the determination of the parameters, which are more difficult to measure and which are not recorded during routine helicopter operations.

The neural network represented functional relations between different types of load $R_{load\text{-}i}$

$$R_{load\text{-}i} = f_i(V_x, V_z, \alpha_w, \Theta_x, \Theta_y, \varphi_o)$$

and components of the free flow at the rotor disc(horizontal V_x and vertical V_z,), angle of rotor shaft inclination α_w, swash-plate bank angle θ_x and pitch θ_y as well as blades collective pitch φ_o .

The following ranges of parameters were assumed:

- horizontal airspeed V_x from 60 up to 230 km/h;
- vertical speed V_z from – 4 up to 4 m/s;
- pitch angle of the rotor shaft α_w from –10° up to 8° ;
- bank angle of the swash-plate θ_x from –4.5° up to 1.5° ;
- pitch angle of the swash-plate θ_y from –6° up to 6° ;
- rotor blades collective pitch φ_o from 14° up to 26°.

The loads were estimated for a model of the isolated rotor under quasi-static conditions with its 3D position unchanged.
In each case numerical simulations were performed for the interval corresponding to nine rotations. The first eight rotations allowed for the decay of initial conditions. The results of calculations for the 9th rotation were accepted as the input data for neural network training.

The results of calculations made using the trained neural network with the defined amplitudes and mean values of blade control moment and bending moment of the rotor hub body are presented in the figures. The scatter can be seen between the calculated results and the real values.

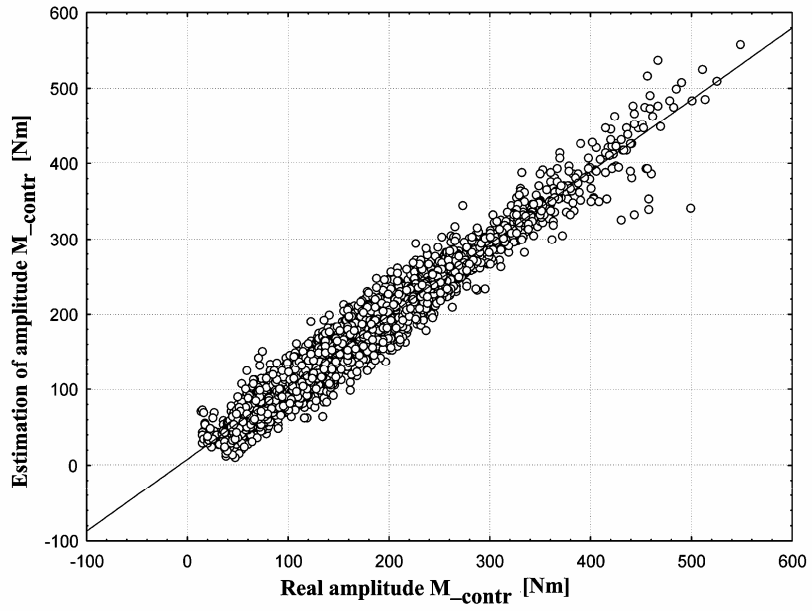

Fig. 2.6.1. Blade control moment amplitude. The scatter between the calculated results (the neural network) and the real values.

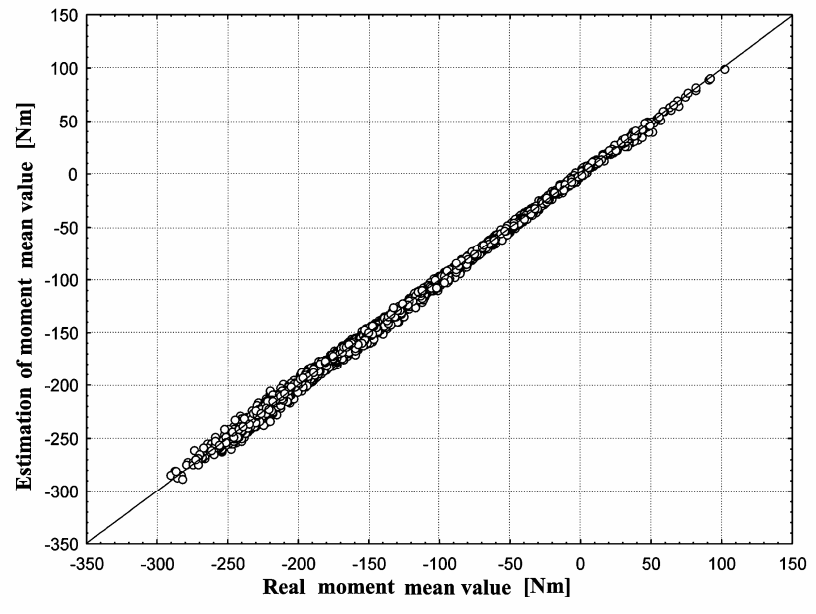

Fig. 2.6.2. Mean values of bending moment of the rotor hub body. The scatter between the calculated results (the neural network) and the real values.

3. AIRPLANE STRUCTURES

3.1 Further Fatigue Tests of the PZL M28 05 SKYTRUCK Empennage

(Janusz Pietruszka – PZL-Mielec)

After obtaining promising results from the previous fatigue tests made on the PZL M28 05 SKYTRUCK empennage at the Structural and Component Test Laboratory of the Institute of Aviation in Warsaw (see reports in *Review of Aeronautical Fatigue Research and Development in Poland During the Period 1999 to 2002*), in which 40000 flight hours were simulated, it was decided that the test should be continued at the Structural Tests Laboratory of Polskie Zaklady Lotnicze in Mielec. The empennage with the rear part of fuselage was transported from Warsaw to Mielec. The same test program was applied using a safe life approach. The test stand was built to ensure that the same loads were applied to the test article and the same reactions appeared (see Fig. 3.1.1). Hydraulic servo actuators were controlled by a computer system developed in Mielec. The same strain gauges were used in monitoring the stress level in critical points of the structure, mainly in a stabilizer torsion box (see Figs. 3.1.2 and 3.1.3). The goal of test was to reach the service life of 16000 flight hours. With a scatter factor of 4, the total number of 64000 flight hours should have been simulated, so that 24000 flight hours were to be simulated in Mielec.

The results obtained in view of both the stresses and deflections were very close to those obtained in Warsaw. After simulation of 6356 flight hours (in fact, after 46356 flight hours, including the previous test in Warsaw) a crack was observed in a stabilizer in the region of front spar lower cap, close to rib No. 1 (attachment to the fuselage, right-hand side, see Fig. 3.1.4). Despite the relatively low stress level observed, this region was predicted in previous fatigue analysis as a critical due to geometric stress concentration. The test was stopped and the damaged region was subjected to a more detailed inspection. More short cracks were found not only on the lower cap, but also on the upper one. The symmetry may be explained by the applied load spectrum, which is symmetrical since the ground loads during operation on an unpaved air strip are predominant in the fatigue damage evaluation. The material of failed spar caps was examined as well, i.e., the D16chT aluminium alloy of upgraded strength (a chemical constitution as 2024) with the following strength parameters for 2 samples: Ftu = 572 MPa and 559 MPa (minimum according to the standard is 470 MPa), Fty = 448 MPa and 441 MPa (minimum according to the standard is 355 MPa) and A50 = 13% and 12.5% (minimum according to the standard is 8%).

The stabilizer front spar in a central region occurred to be a weak area and it was decided that it should be modified. The cap cross-section surface was significantly enlarged and the stress

concentration due to the spar plane bending of rib No. 1 was minimized. The structure modified in such a way will be subjected to further testing.

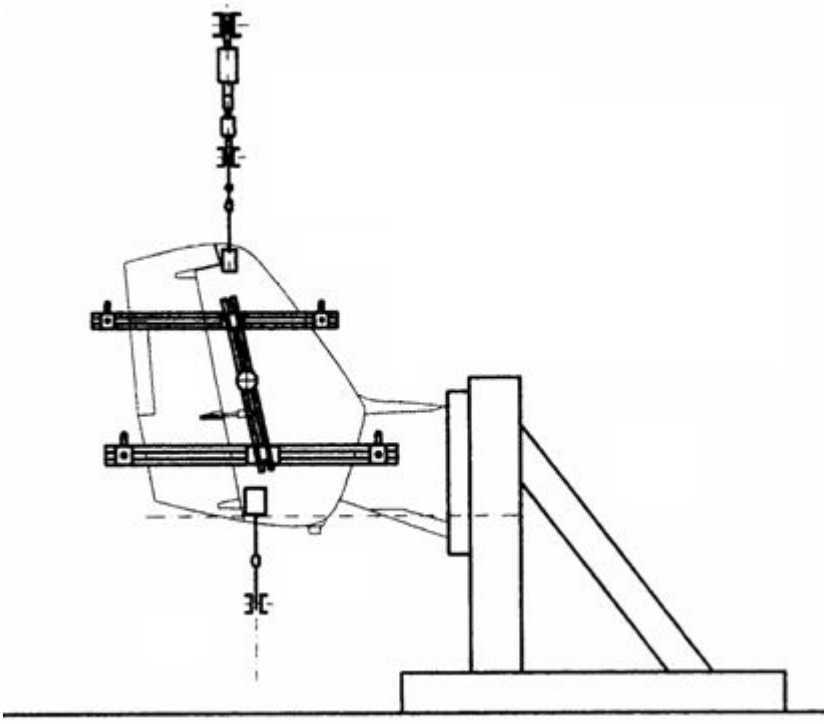

Fig. 3.1.1. The side view of a test stand with the PZL M28 empennage (with a double vertical tail) and the rear part of the fuselage.

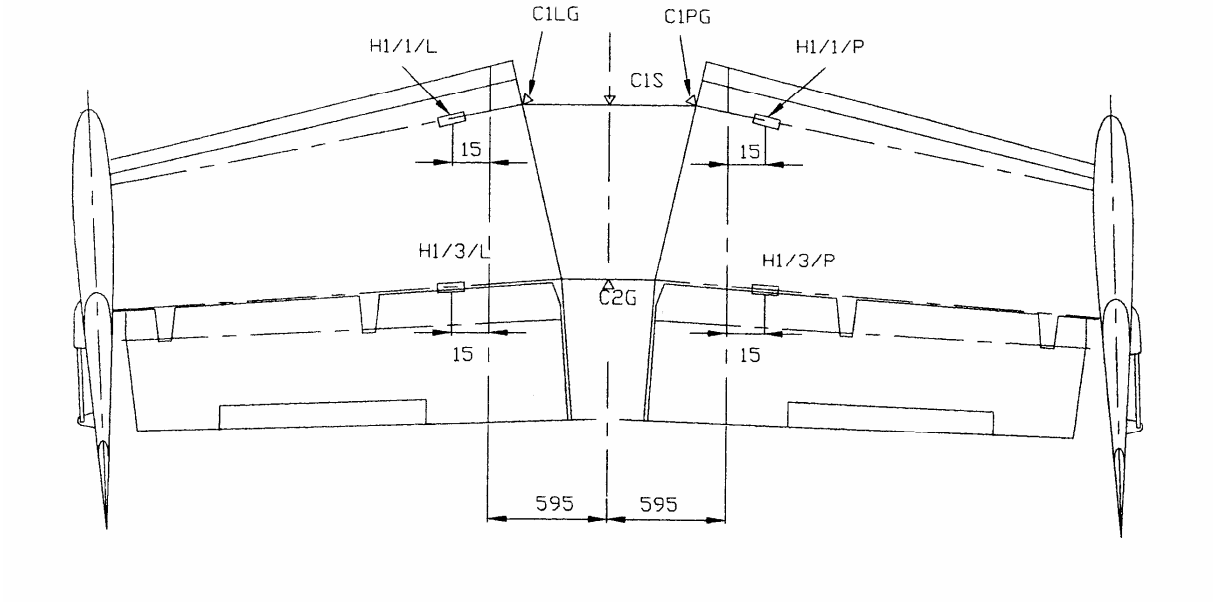

Fig. 3.1.2. The upper view of strain gauges located on a horizontal tail (stabilizer).

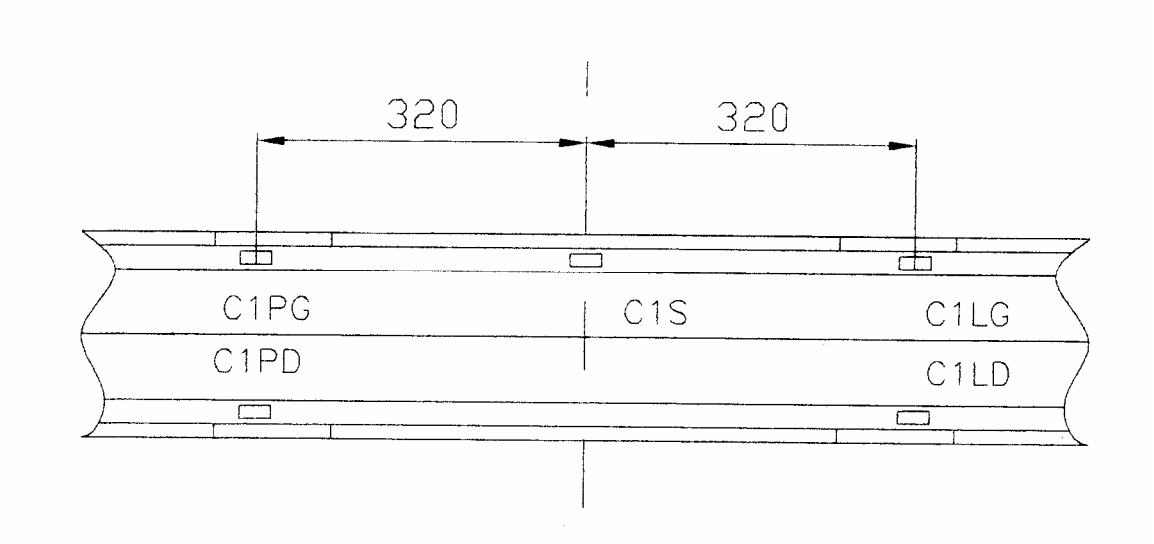

Fig. 3.1.3. The front view of the stabilizer front spar with strain gauges.

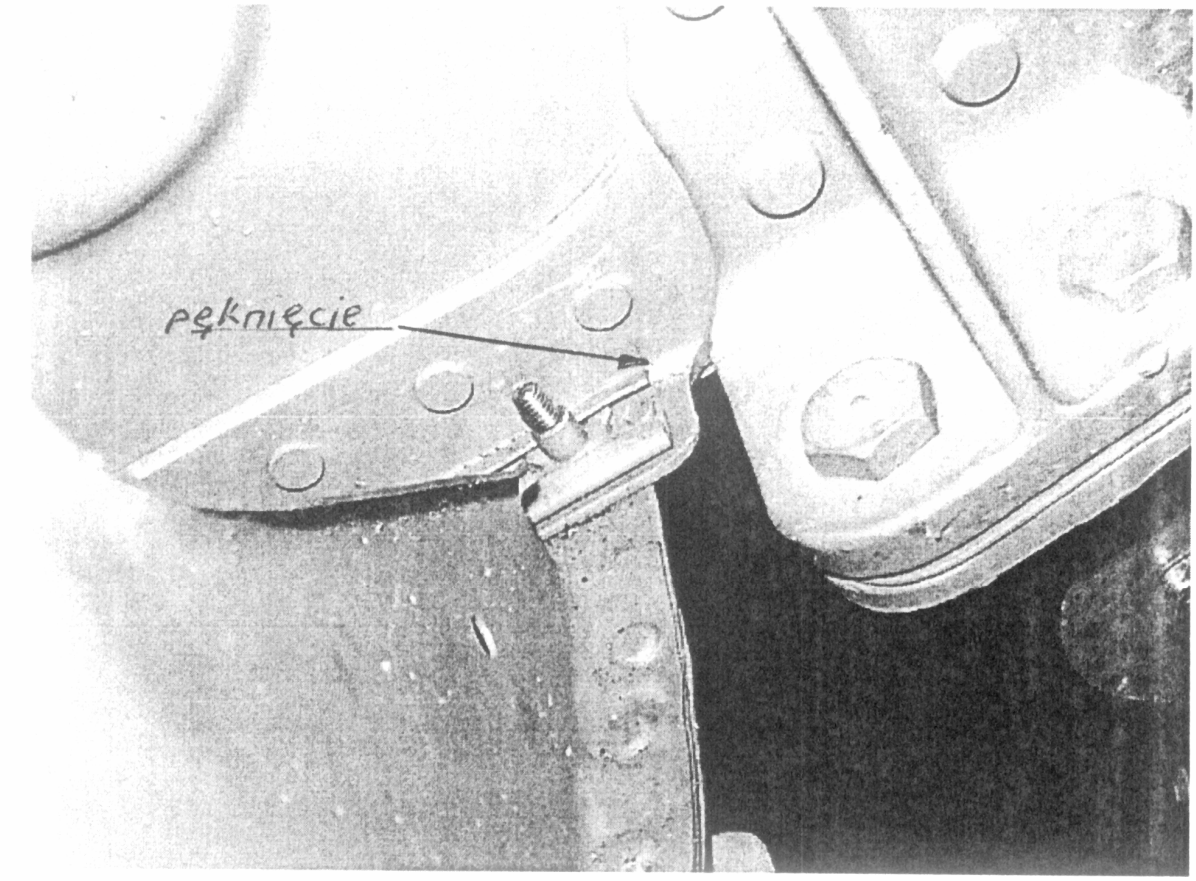

Fig. 3.1.4. The photo of the stabilizer region with a crack (indicated by an arrow) observed during the test.

3.2 Full-Scale Fatigue Test of Commuter Aircraft Nose Landing Gear Made of High Strength Low-Alloy Steel

(Janusz Pietruszka – PZL-Mielec)

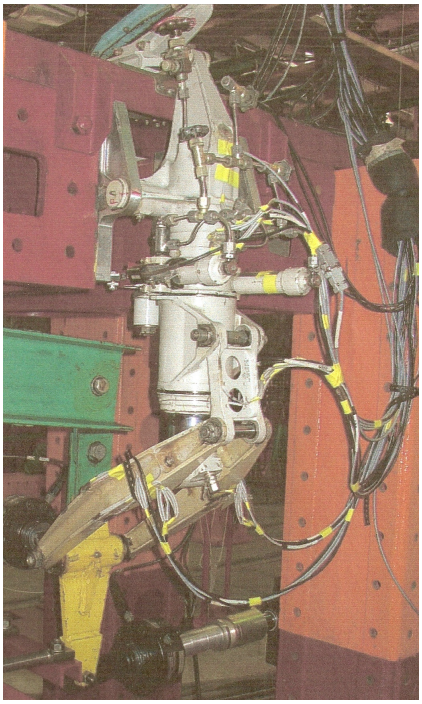

To determine the service life of PZL M28 Skytruck commuter aircraft undercarriage, full-scale fatigue tests were performed at the Structural Tests Laboratory of PZL Mielec. The aircraft is designed for operation on normal and grass airfields. Its maximum take-off and landing weight is 7500 kg (16535 lbs.). The undercarriage is a fixed, tricycle type. It is made from two high strength low alloy steels - 30HGSA and 30HGSNA. Fatigue failure of the main landing gear was observed in a relatively short time. Since no severe damages of the nose landing gear had appeared, it was decided to continue the test of nose landing gear up to reach the service life of 16000 flight hours. Having assumed the scatter of 4, the total number of 64000 flight hours should be simulated.

Fig. 3.2.1. PZL M28 nose landing gear fatigue test stand.

The MTS Aero 90-LT loading system was used with three loading channels (vertical force, side force, and fore and aft force) and 18 monitoring channels. Twenty strain gauges there were glued onto the leg, rocker arms and other parts in order to monitor integrity of the structure at the most severe stressed points, and to verify the calculated stress levels. The most closely observed region was the sharp bend of gear lever arms, considered to be critical.

During the test a crack was observed at the fitting that connected the lever arms with the cylinder. The test was conducted further on since the landing gear was still capable of withstanding the applied loads. After 3000 simulated flight hours the test was stopped and the fitting was replaced with the another one of the same design. Once more a crack occured, therefore the fitting was redesigned and a modified design was then tested. Both the fittings are shown in Fig. 3.2.2. The test on the new fitting was conducted up to 64000 simulated flight hours without any other cracks.

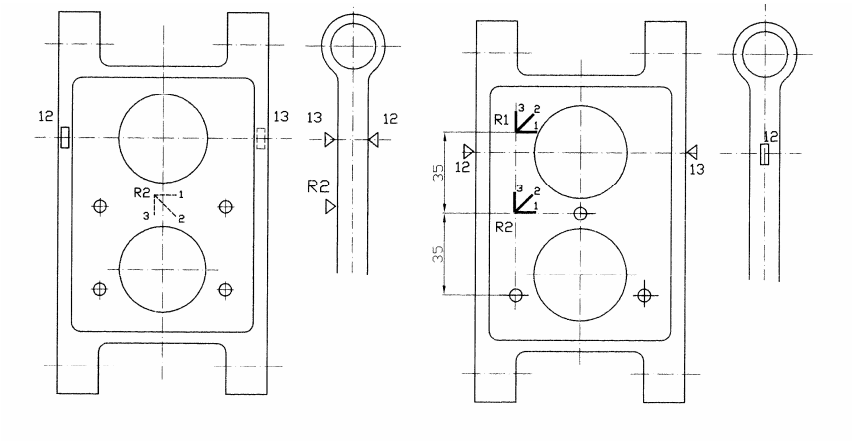

Basing on the test results the service life of investigated nose landing gear has been determined as 16000 flight hours on condition that the modified fitting is used.

Fig. 3.2.2. Fitting that connects the lever arms with the cylinder of nose landing gear. On the right-hand side the initial design is shown. Two times during the tests a crack occurred at a

little hole between the big holes, in the central part of fitting. On the left-hand side the modified design is presented.

3.3 Non-Destructive Inspection of Selected Elements of the SMG-92 TURBOFINIST Aircraft

(Józef Krysztofik – Institute of Aviation)

Elements of the SMG-92 TURBOFINIST aircraft No. HA – YDK (Fig. 3.3.1) after „a hard landing" were investigated.

Fig. 3.3.1. Aircraft SMG – 92 TURBOFINIST.

As a result of the "hard landing", the undercarriage legs were permanently deformed. A non-destructive inspection was performed in order to verify that no damage had occurred in other elements of the aircraft structure.
The following elements of the structure were chosen:

- wing fittings,
- wing strut fittings,
- undercarriage leg fittings,
- undercarriage bearing rings,
- undercarriage leg fitting attachment bolts,
- strut fittings of the empennage,
- all welded joints of the engine mounting,
- fitting attachment zones.

The magnetic particle method was employed. Some elements were made from nonmagnetic material, therefore, the eddy current method was also applied.

The following test equipment was used when following the magnetic particle method:

- magnetic defectoscope MAGNAFLUX Y6 ELECTROMAGNETIC YOKE made by Magnaflux Corporation, USA,
- standard indicator control blocks, MAGNAFLUX Type 008M005 A (Aero-space), acc. to BS 6072 and EN ISO 9934,
- magnetic suspensions, MAGNAFLUX 7HF MPI Ink, USA,
- test block, the Institute of Aviation (IA),
- white light source (BW-W61 I.A.).PL.

while, in the course of eddy current investigation method the test equipment was as follows:

- eddy current defectoscope, typ Defectometer H 2.835made by Dr Foerster Institute, Germany,
- probe Fe: Fe 2.835.01-3500, Fe 2.835.01-3600,
- probe NFe: NFe 2.835.01-2000, NFe 2.835.01-2100, NFe 2.835.01-2600,
- standard test block; Foerster type Fe 2.164 - 501,
- standard test block; Foerster type NFe 2.164 – 551.

During the investigations conducted all hinges, except for the undercarriage fuselage fittings were remained on the aircraft while the undercarriage leg fuselage fittings, fitting bolts and bearing rings were disassembled.

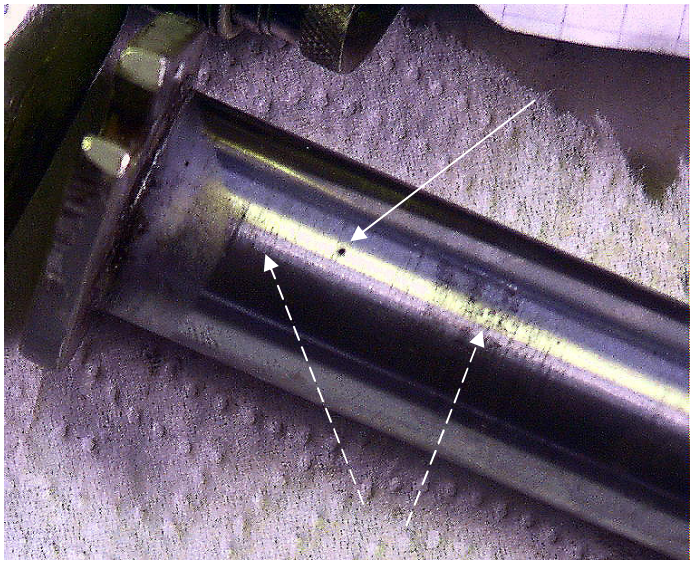

Fig. 3.3.2. Landing Gear, right leg, fuselage fitting fixing bolt.
The material defect of pinhole type – (full line);
circumferential scratches on the surface - (dotted line).

As a result of the inspection the following two recommendations have been formulated:

1. Replacement of the right leg fitting bolt. In the region the material defect of pinhole type was detected, which could initiate a fatigue crack. So as the scratches and the traces caused by strokes – indentations.
2. Avoiding scratching of the bolts surface, which could result in fatigue crack initiation.

Additionally, the sharp, non-smoothed edges were detected at the bolt holes of left and right legs fittings, which formed a notch.

3.4 Load Database Development for the Fatigue Analysis of MIG-29 Structure

(Mirosław Nowakowski – Air Force Institute of Technology)

The investigations aimed at the development of load database in some selected structural elements of the MIG-29 aircraft. Measurements of loads affecting the MiG-29 structure were taken with use of the KAM-500 system.

The scope of flight tests comprised the following elements:

a) test after the installation of KAM-500 system,
b) engine test,
c) ground handling along the runway and taxiways,
d) touch-and-go landing, landing at increased speed, afterburner-assisted take-off,
e) straight-and-level flight,
f) level flight at bank angles lower than 90^0 both to the left and to the right,
g) level flight with rolls:
- slow half-rolls and rolls at the angular speed of $30 \div 35^0$/s,
- flick half-rolls and rolls at the angular speed of $50 \div 60^0$/s,

h) climb-forward flight,
i) climb-forward flight at bank angles lower than 90^0 both to the left and to the right, the angle of pitch $20 \div 30^0$,
j) climb-forward flight with rolls at the flight ascending path angle of $10 \div 30^0$:
- slow climbing half-rolls and rolls at the angular speed of $30 \div 35^0$/s,
- flick climbing half-rolls and rolls at the angular speed of $50 \div 60^0$/s,

k) climb inverted flight,
l) descending straight flight,
m) descending flight at bank angles lower than 90^0 both to the left and to the right,
n) descending flight with rolls:
- slow downward half-rolls and rolls at angular speed of $30 \div 35^0$/s,
- flick downward half-rolls and rolls at angular speed of $50 \div 60^0$/s,

o) descending inverted flight,
p) aerobatic manoeuvres (turns, divings, pull-ups, loops, climbing turns, hammer-head stalls, Immelmans, hammer-head semi-stalls).

The load spectra were recorded and stored in the database of the Air Force Institute of Technology. The results obtained from both the flight tests and analysis will contribute to the extension of the MiG-29 service life.

3.5 Static and Fatigue Tests of the Fan-Cowl A318 Hinge Fitting and Latch Housing

(Sebastian Szałkowski – Institute of Aviation)

Static and fatigue tests of hinge fitting and latch housing of the A318 fan-cowl were carried out at the Institute of Aviation to the order of EADS CASA in Madrid.
Each test specimen consisted of hinge fitting or latch housing joined to a representative panel (two panels in the case of latch housing specimen) of the surrounding area, including beams and stiffeners. Two similar specimens of each element were manufactured, one for static tests and the other for fatigue tests. The specimens were made mainly from steel and aluminium alloys.

The Institute of Aviation designed and built the test set-up and installed the hydraulic loading system, the control system and the measurement and the data acquisition system. The entire test set-up for each specimen consisted of a specimen fixing frame and a one-channel load application system. Fig. 3.5.1. shows the test set-up with the hinge fitting specimen (one of the configurations) and Fig. 3.5.2. shows the test set-up with the latch housing specimen. 137 channels for the strain gauges and 3 displacement transducers for both specimens were required to measure the specimen behaviour during both the static and fatigue tests.

Fig. 3.5.1. Test set-up with the hinge fitting specimen.

The static tests were performed up to the limit load and to the ultimate load and then to the specimen failures. Both the specimens successfully withstood the required limit and ultimate loads, respectively.
The fatigue tests consisted of the following three phases: fatigue, damage tolerance and residual strength testing, respectively. In total, both the specimens were subject to 192 000 fatigue cycles (FC), which corresponded to three service lives and 22 500 cycles under the

damage tolerance conditions (DTC), which corresponded to three inspections intervals, respectively. The inspection program included visual inspections every 8 000 FCs at the fatigue phase and every 3750 DTCs at the damage tolerance phase while the non-destructive inspections (high frequency eddy current method) were made every 32 000 FCs at the fatigue phase and after each inspection interval (7500 DTCs) at the damage tolerance phase. Visual inspection intervals were shortened to every 1500 DTCs at the damage tolerance phase in the course of hinge fitting tests due to the crack appearance at this phase. Both the specimens withstood successfully the limit loads during the residual strength test after the damage tolerance phase.

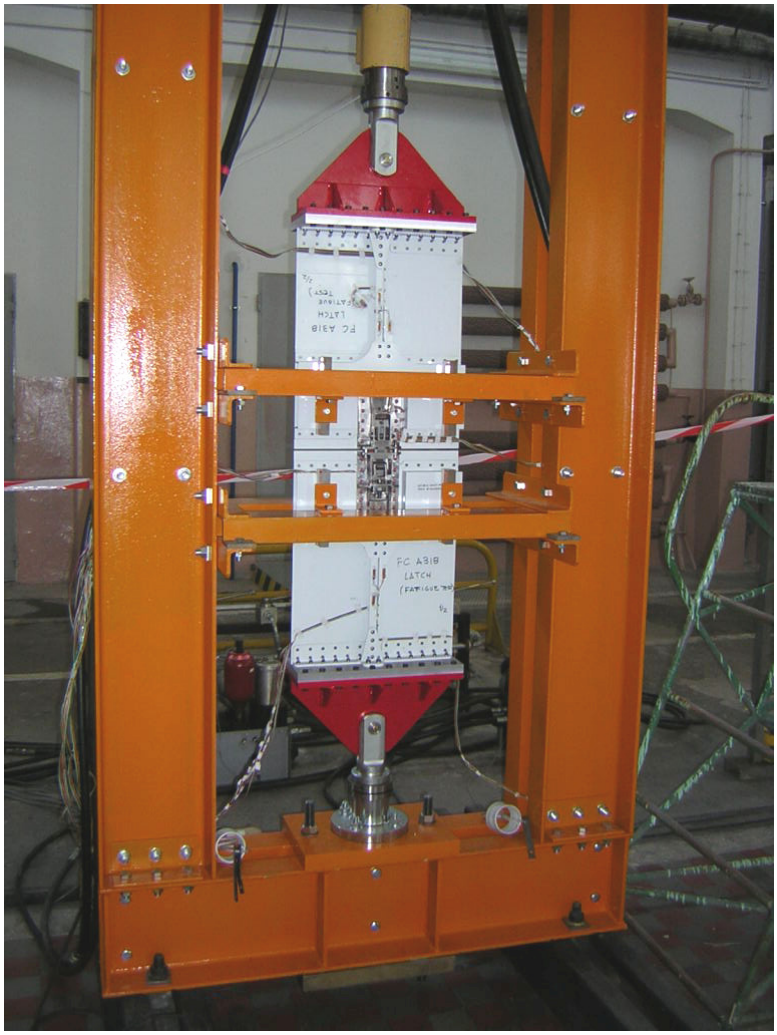

Fig. 3.5.2. Test set-up with the latch housing specimen.

3.6 Fatigue Test of Composite Wing Spar

(Sebastian Szałkowski - Institute of Aviation)

The fatigue test of a composite wing spar of the I-23 *Manager* aircraft was carried out at the Institute of Aviation in Warsaw. The I-23 *Manager* (Fig. 3.6.1) is a small business aircraft with four seats developed by Institute of Aviation. The aircraft is made of glass and carbon fibre composite materials. The wing spar is made of carbon fibre reinforced plastic (CFRP) with metallic fittings for joining two halves of the spar in the symmetry plane of the aircraft, and for attaching the spar to the fuselage and for attaching the main landing gear.
In the test the wing spar was attached to the dummy representing a third fuselage frame and supported to avoid undesirable torsional deflections. Due to skin contribution in loads transfer to accurately simulate the operational loadings and stress distributions spar loads were separated from the wing loads using the FEM approach. The test loads were applied by a 4 servo-hydraulic actuators and introduced in 3 sections of each half of the spar i.e. at ribs 7 and 9 and in the landing gear fitting. Fig. 3.6.2 shows the entire test set-up. During the fatigue test, data on the load, strains and deflections were recorded every 1000 flights.
The test was carried out at room temperature and without moisture conditioning. Some artificial defects e.g. bonding failures were introduced into the CFRP structure. The inspection program included both visual and NDT inspections with periodical wing spar disassembly to examine the central fittings. A flight-by-flight loading spectrum was applied. 40000 flight hours (which correspond to 4 design service goals) were successfully simulated until December 2006.

Fig. 3.6.1. I-23 Manager aircraft

Fig. 3.6.2. Wing spar test set-up.

3.7 Crack Initiation and Fatigue Life Analysis of the Aircraft Wing-Fuselage Connector

(Lucjan Witek- Rzeszow University of Technology)

The wing-fuselage connector, which joins the wing spars to the fuselage bulkhead, is one of the most critical aircraft parts. It transmits aerodynamic, inertial and gravity forces from the wing to the fuselage. Its life often limits the service life of the entire airframe due to large operational loads. The aircraft structural elements are often exposed to hot, humid and polluted air during agricultural operations. Working under conditions of atomized chemicals exerts also negative influence on the fatigue life of the airframe elements. Corrosion can affect the aircraft structural integrity since the fatigue cracks can initiate from corrosion pits and grow at an accelerated rate in the corrosive environment.
The problem of premature fracture failure of the wing-fuselage connector occurred in a certain type of agricultural aircraft after about 5000-6000 hours of operation. The connector failed due to the fact that an undetected fatigue crack in the lower lug had reached the critical size. In three cases the connector failure was the reason for the crash. After these accidents, the producer of aircraft ordered detailed inspection of the connectors in all planes after 3000 flight hours. In a few cases both corrosion pits and small cracks were detected in the lugs of aircraft after 4000-5000 flight hours in total. In most cases these problems were reported to the producer. As a result, the producer modified the connector. This modification consisted in enlarging of the lug hole with a small corner crack by means of drilling. The hole was then filled with an additional intermediate sleeve. This modified connector has been tested in the laboratory. The fatigue life of the modified connector was almost four times longer than for the previous design.
The research was focused on the explanation of reasons for such a considerable increase of the fatigue life and also the reasons for the premature failure of the original connector.
The commercial finite element programs: MSC Patran 2005, AFEA and MSC Fatigue v.9.0 were used for solving the problem.

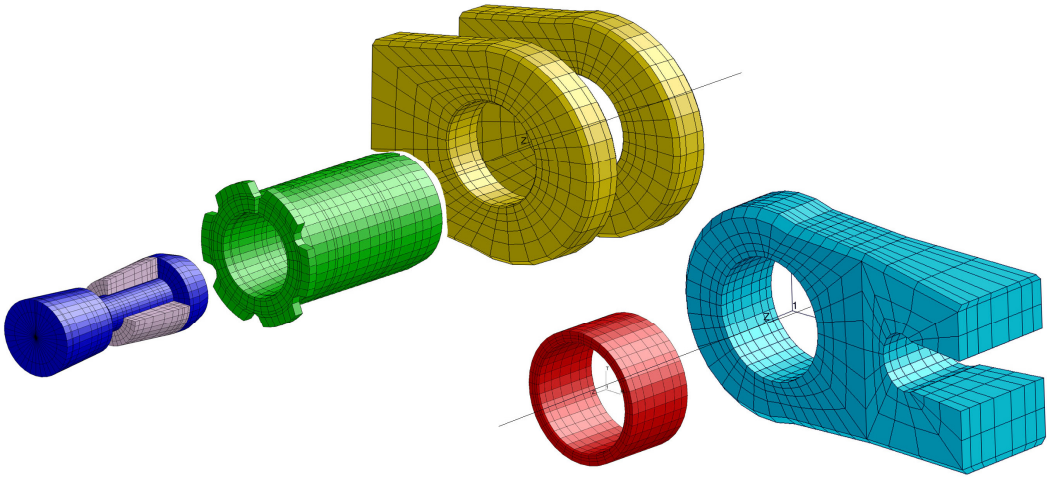

Fig. 3.7.1. Components of the numerical model of connector before assembling.

The stress contours were generated basing on the results of nonlinear static analysis conducted for both the standard and modified connectors, (Fig. 3.7.1) under operating conditions. Zones

of high stresses were found at the region of wing lug, where the cracks were detected in the aircraft (Fig. 3.7.2).

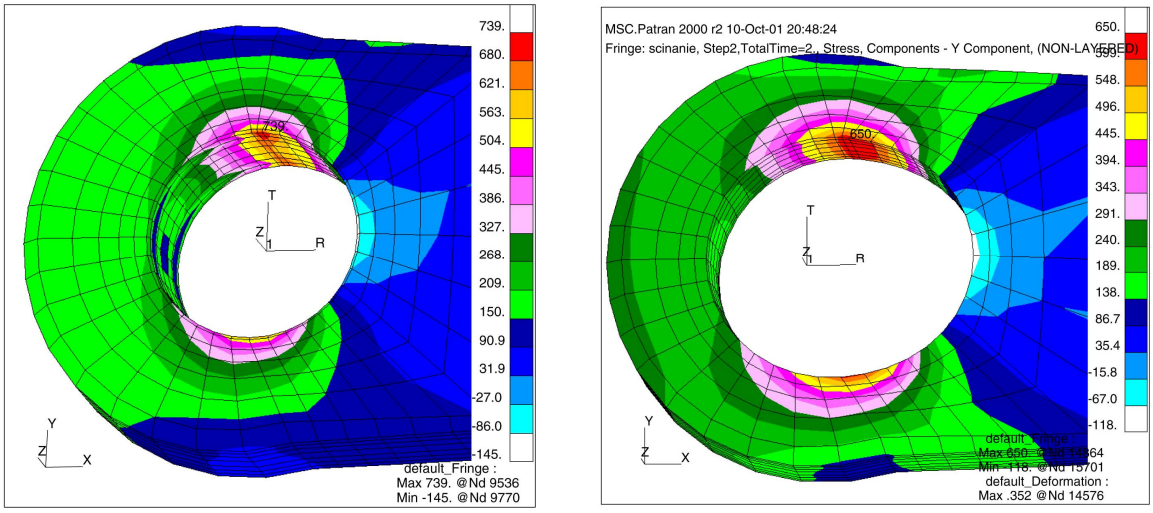

(a) (b)

Fig. 3.7.2 Circumferential stress distributions in the original lug (a) and after modification (b).

The results of total fatigue life (S-N) and crack initiation (ε –N) numerical analysis, conducted for the load history corresponding to 10-minute operating flight of the agriculture aircraft are presented as well. In this analysis, the number hours of flight before the first fatigue crack and also before a total damage of the critical part of connector were estimated.

The results of ε –N analysis for the original wing lug are presented in Fig. 3.7.3a. From the figure it can be seen that the minimum number of hours before the first fatigue crack (for depth of crack at about 1,5 mm), equals $10^{3,6024}$ =4003 hours of flight.

Fig. 3.7.3b presents the results of the ε-N analysis for the modified wing lug. From this figure it can be seen that in the modified lug the first fatigue crack can occur after $10^{3,96}$ = 9120 hours of flight.

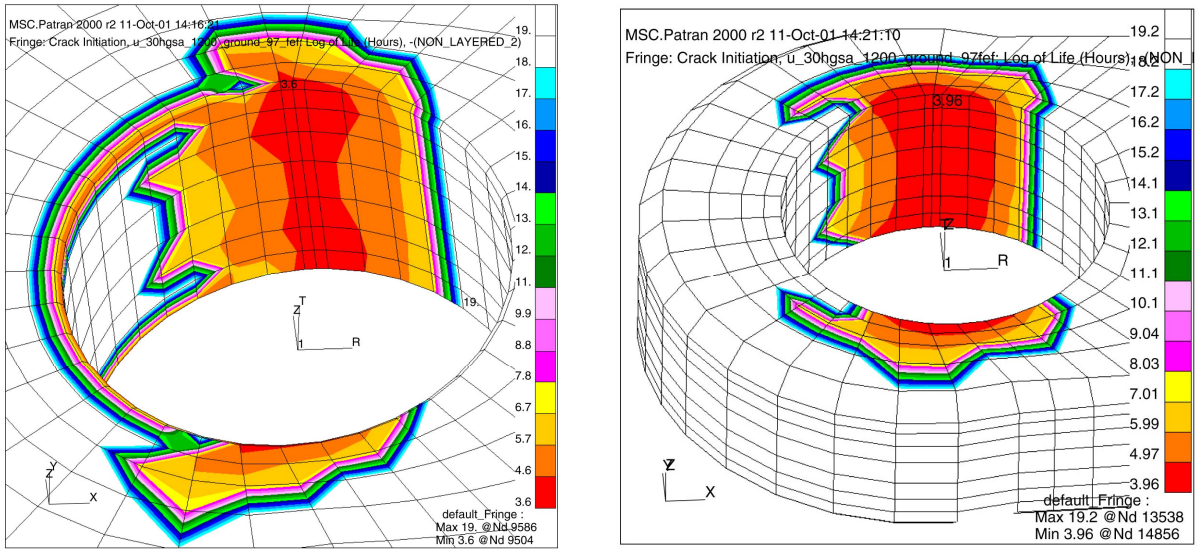

a) b)

Fig. 3.7.3. Results of ε-N analysis – number of flight hours to first crack initiation and location of the fatigue critical region for original (a) and modified (b) wing lugs

4. MATERIALS TESTING

4.1 Investigations into the CFRP Strength Deterioration due to Fatigue Loads or Impacts

(Mirosław Rodzewicz, Anna Boczkowska – Warsaw University of Technology)

Part 1

The influence of low-cycle fatigue loads on compressive strength of the CFRP- UD composites, and on signal variation in the ultrasonic structural tests

The increasing application of CFRP in constructions subjected to high loads is observed during the last decade. High-performance competition gliders can serve as an example. When the level of operation loads is very high – even small damages of the composite structure may narrow considerably a margin of safety. That was the reason behind undertaking the investigations into sensitivity of the CFRP composites to fatigue and impact loads. In the research the attention was focused on composites with uni-directional (UD) structure. Such composites are used in the wing spar flanges (cups). Those elements of the glider structure are subject to highest loads. The compressive strength was investigated since it should be considered as a predominant factor in the wing spar dimensioning.
Two experiments were made. Experiment no 1 was aimed at :

- examination of the influence the low-cycle fatigue loads exert on the residual strength
- comparison between ultrasonic A-scans taken at different stages of the experiment.

The upper magnitudes of loads (see Fig. 4.1.2) correspond to the limiting operational glider loads (G-load equal to + 6g, i.e. the magnitude appearing due to a strong vertical gust), while the lower ones correspond to the G-load equal to +1 (i.e. for a horizontal flight at smooth air). The assumed number of cycles applied was 10 000. Experiment No 2 was aimed at finding the moment of fatigue test made with increasing load levels, at which structural changes of the CFRP appear, introducing changes into the A-scans. The specimens were made of: carbon roving: Tenax 5631HTSA; epoxy resin & hardener: L285/286. The volume fraction: 0,46; thermal cycle: 24h – RT plus 15h at 60°C.

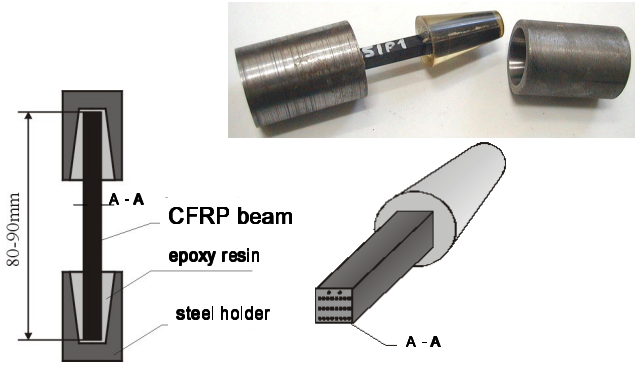

Fig. 4.1.1. Specimen used for the static and fatigue compression tests.

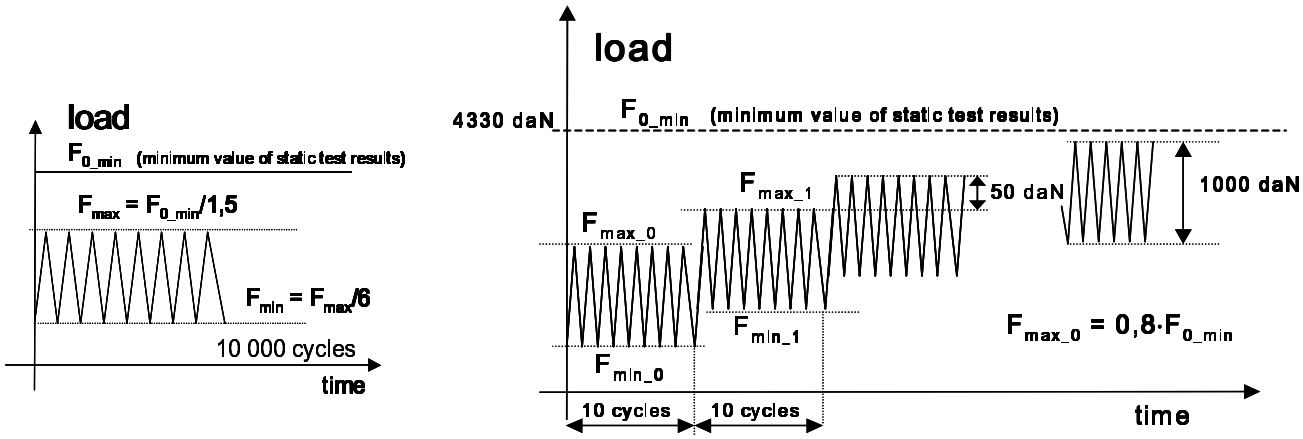

Fig. 4.1.2. Profiles of the fatigue loads in Experiment No. 1 (left) and Experiment No2 (right).

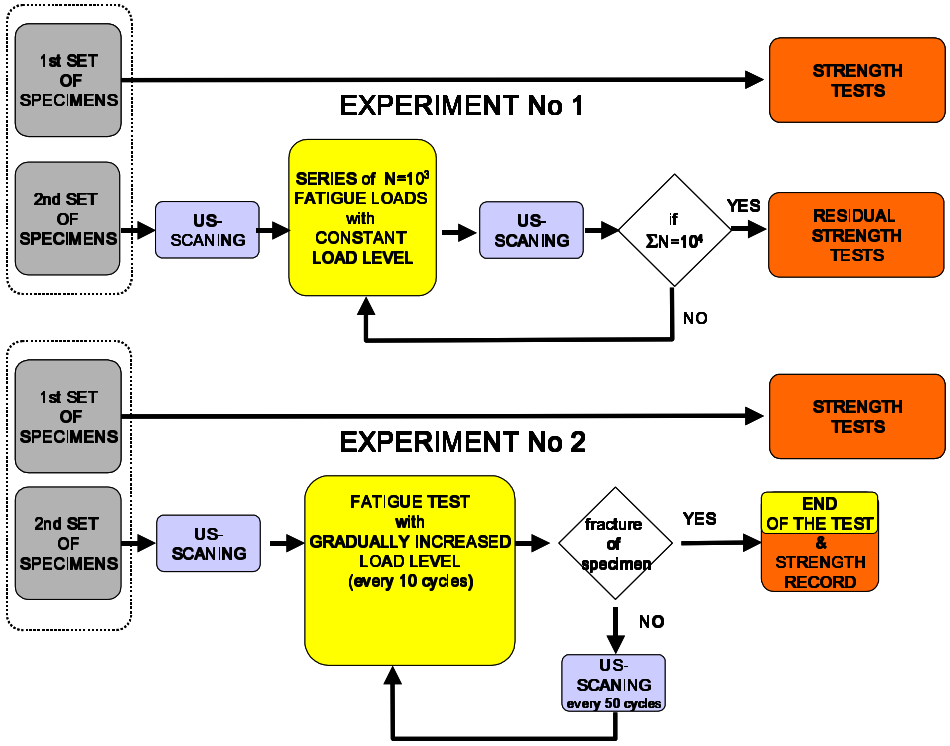

Fig. 4.1.3. Block-scheme of the low-cycle fatigue testing.

The ultrasonic investigations were conducted on the immersion stand, equipped with ultrasonic flaw detector Panametrics 9100 connected to a PC. The results of static and the residual strength tests obtained from Experiment No 1 are illustrated in Fig. 4.1.4.

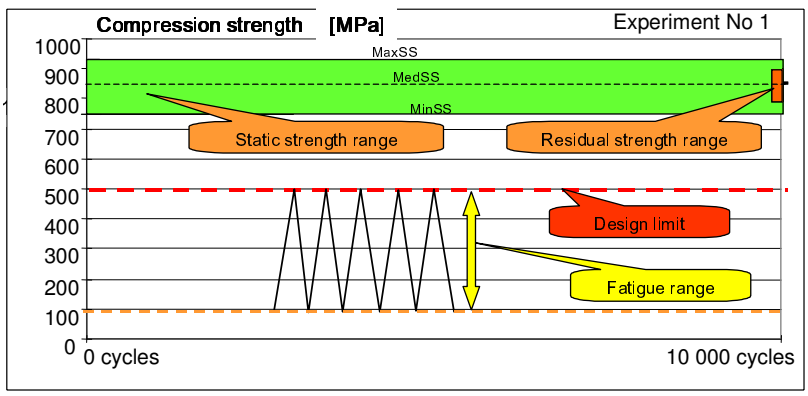

Fig. 4.1.4. Set of the static and the residual strength ranges after 10 000 cycles.

It can be seen from the figure that the results are situated within the range of static strength scatter. Which was due to the fact that no significant changes, which might affect the strength appeared in the specimen structures. That was also proved by ultrasonic scans, in which no significant differences could be seen.
Basic results obtained from Experiment No 2 are shown in Fig. 4.1.5. The fatigue tests were made up to the lower strength limit of the static strength range. At several phases of the test the specimens were examined on the ultrasonic stand. Every scanning session was performed for several available filter-frequencies. No significant differences in the A-scans were observed.

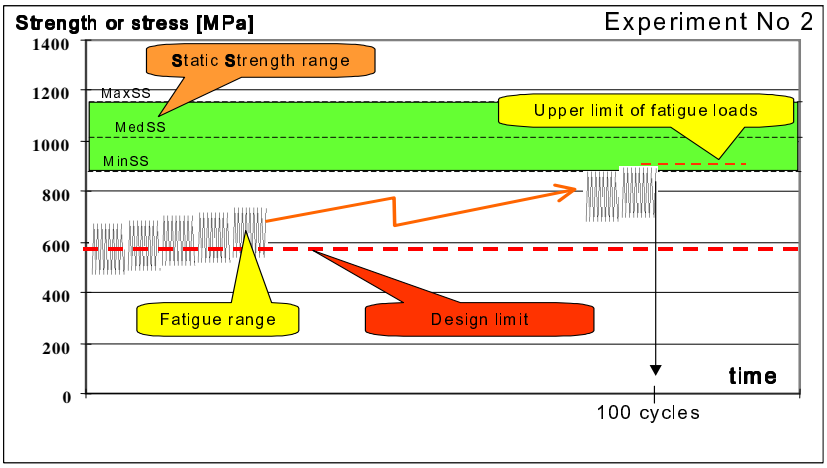

Fig. 4.1.5. Course of thelow-cycle fatigue test in the range of over- limiting operational loads.

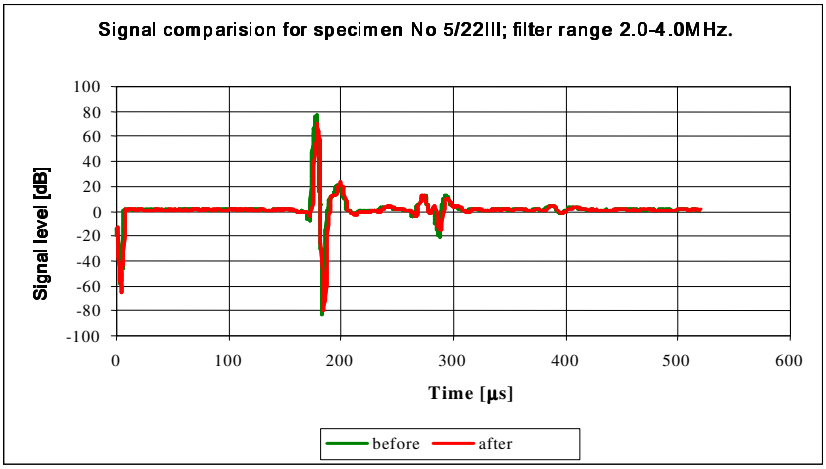

Fig. 4.1.6. Set of the A-scans for initial and final stadiums, respectively, of the fatigue tests (typical diagram for experiments No 1 & 2).

The following conclusions can be drawn from the low-cycle fatigue test results:

- The low cycle fatigue loads did not cause strength deterioration in the applied range of loads
- The similarity of ultrasonic A-scans taken in the initial and final stadiums of the fatigue tests have proved that no significant changes appear in the CFRP structure within the applied range of the loads;
- The process of destruction develops rapidly after exceeding a certain level of loads within the range of the CFRP static strength scatter.

The investigations presented above have proved that fatigue durability of the wing spar does not limit limiting fatigue durability of the whole glider structure, provided that it is made from the CFRP of a UD structure and subject to the aforementioned range of operational stresses.

Part 2
Impact tests of the CFRP-UD composites

The impact tests of the CFRP composites had the following goals:

- Assessment of the impact load influence of on the composite strength;
- Examination of the composite volume fracture influence on impact sensitivity
- Examination of the influence the technological aspects exert on the residual strength of composites in view of:
  - A/ method for specimen fabrication (pressure or free forming)
  - B/ quasi-laminar structure of the composite reinforced by carbon roving, (due to the method for specimen fabrication);

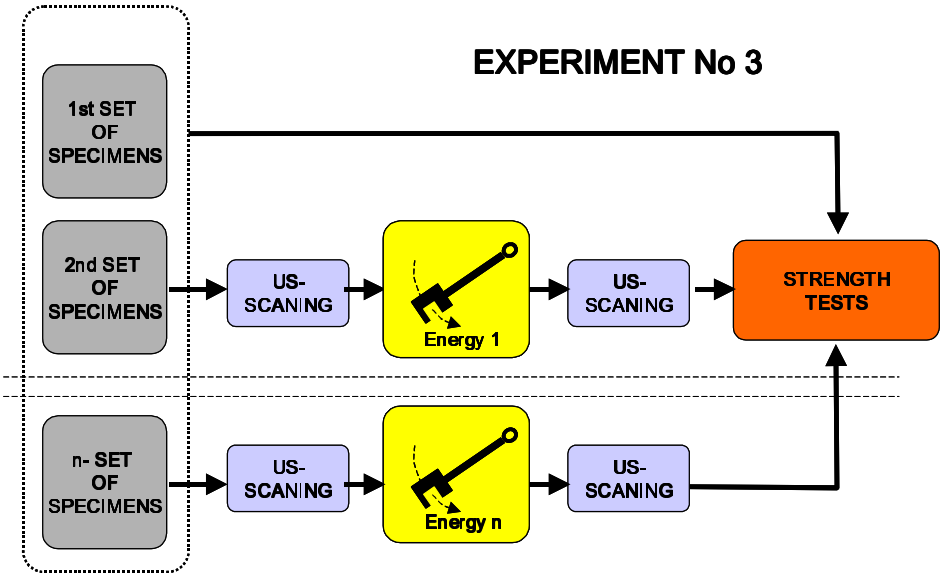

Fig. 4.1.7. Block-scheme of the impact tests.

- Investigation of changes in ultrasonic scans, caused by the impact loads

The Charp method was employed for the impact tests made on CFRP beams. The following values of the volume fracture were applied: 0,36; 0,46; 0,6. The type of resin and thermal profile of a curing process were exactly the same as in the previous part. After the impact and ultrasonic tests the beams were fixed in steel holders used for the strength tests, forming the specimens shown in Fig. 4.1.1.

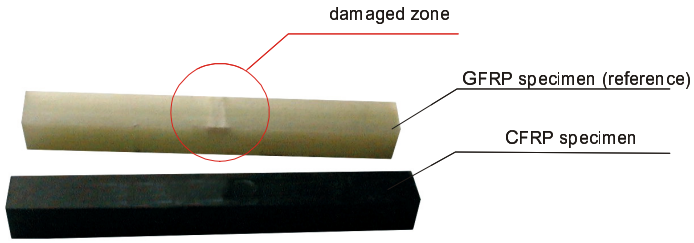

Fig. 4.1.8. Specimens used in the impact tests; (the GFRP specimen was used for better visualization of the impact effect, invisible in the CFRP specimen).

In this case the impact transverse loads introduced significant differences into the ultrasonic A-scans taken in the initial and the final stadiums of the tests (see Fig. 4.1.9). The results of linear scanning (B-scan) are provided as well, with a clearly visible point hit by a hammer. It should be mentioned that it is very difficult to detect such a point using a visual method.

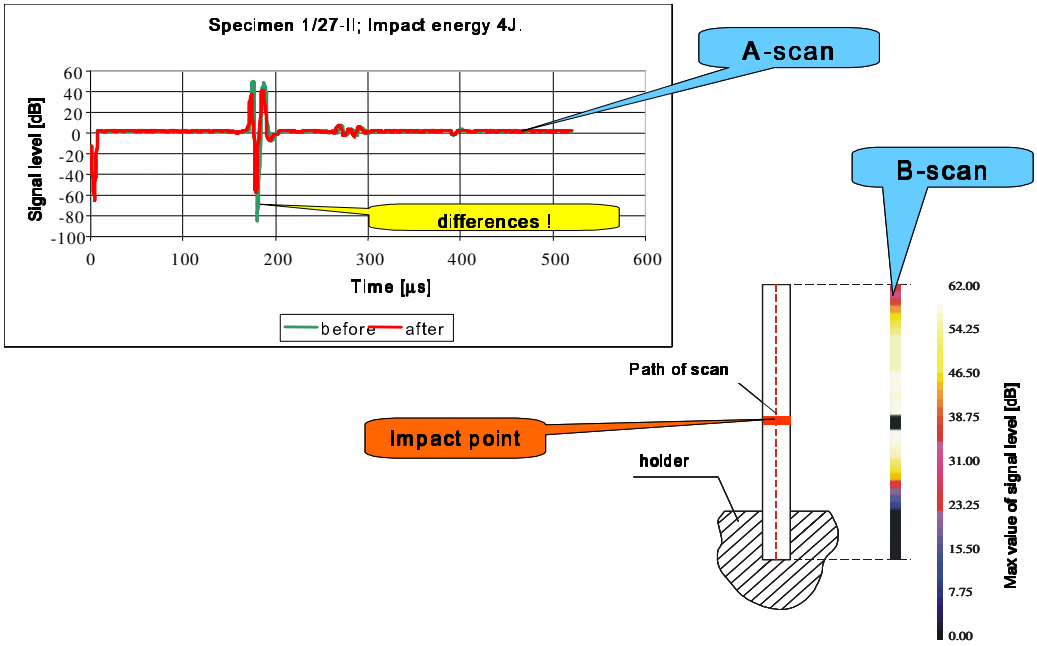

Fig. 4.1.9. A-scans and B-scan of the specimen subject to the impact of 4J energy.

The influence of impact energy on the residual strength is presented in Fig. 4.1.10. together with the results for non-impacted specimens. The diagram reveals the threshold value that separates the ranges of specimen insensitivity to the impact.

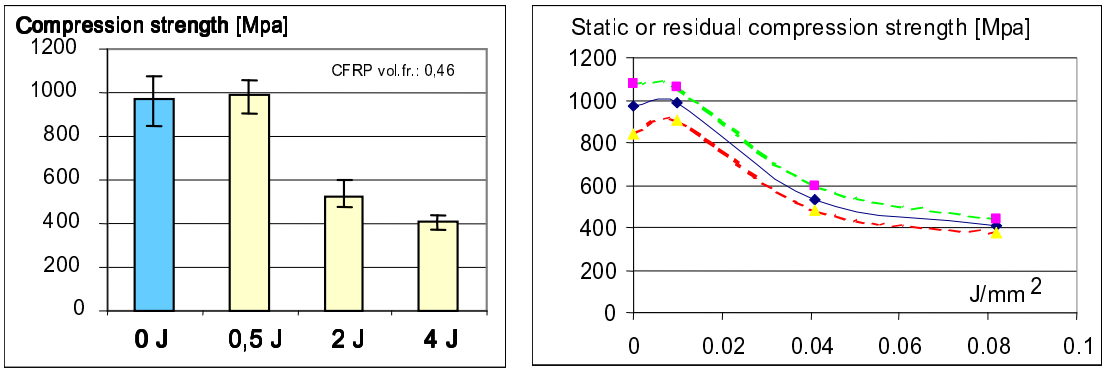

Fig .4.1.10. Impact energy influence on the residual strength.

The volume fracture influence on the residual strength of the specimen subjected to the impact of 2J is shown in Fig. 4.1.11. together with the strength for non-impacted specimens . From the diagram it can be seen, that the highest impact durability of the composite appears close to the volume fracture of 0,5. In the previous investigations it was found that this very value of volume fracture was optimal for the compression strength of the CFRP composites formed using the LPC method.
The influence of technological aspects is illustrated in Fig. 4.1.12. and Fig. 4.1.13. The forming method was taken into account; i.e., free forming (LPC) or pressure forming (HPC). The quasi-laminar structure of the beams reinforced by the carbon roving should be emphasized, caused by the method of beam fabrication; (the strands of impregnated roving are introduced and squeezed in the mould layer by layer).

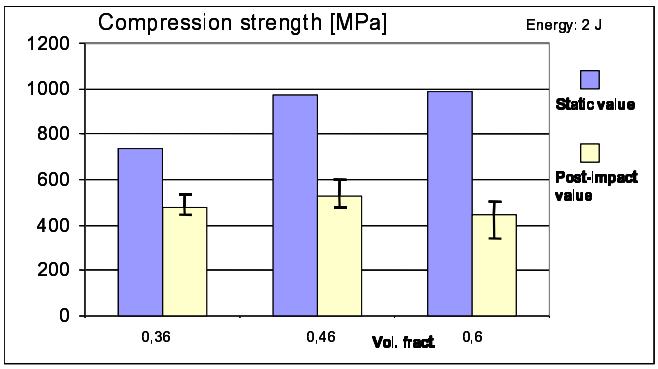

Fig. 4.1.11. Volume fracture influence on the residual strength of the specimen subject to the impact of 2J compared to the static strength at a room temperature.

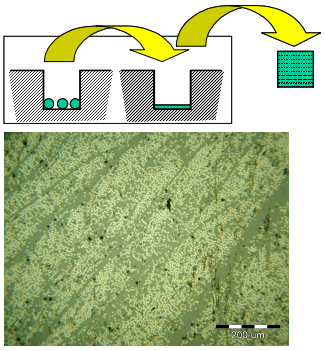

Fig. 4.1.12. Source and the microscopic image of quasi-layers.

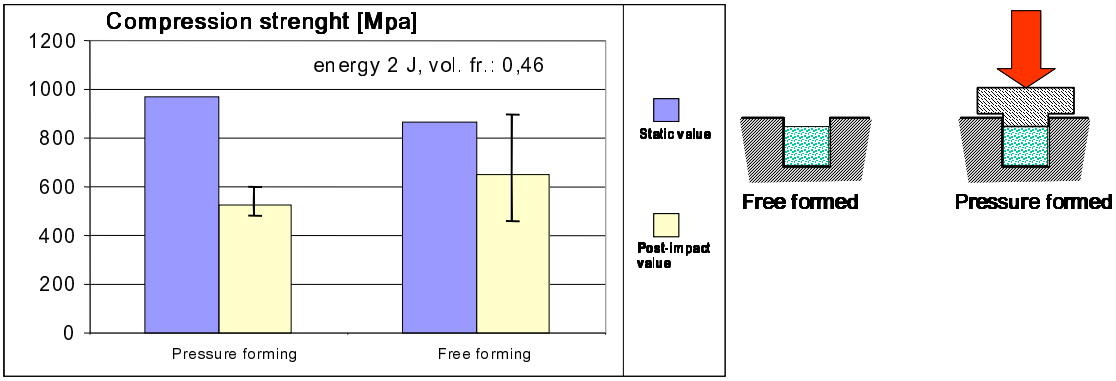

Fig. 4.1.13. Influence of pressure applied during the CFRP beam forming on the static strength and the residual post-impact strength.
From the diagram it can be seen , that the lack of pressure during the beam forming causes wide scatter of the CFRP strength, probably due to higher impact energy dissipation in the structure formed using the LPC method caused by heterogeneity of the structure.

The following conclusions can be drawn from the results of impact tests of the CFRP beams:

- Relation between the residual strength and the impact energy is non-linear revealing a threshold value. Beyond this limit a rapid deterioration of the residual strength of the CFRP can be observed.
- Optimal volume fracture of the CFRP is 0,5 –for both the post-impact residual strength and static compressive strength of the CFRP composites formed without a pressure.
- The quasi-layered structure of the CFRP beams, affected by the manufacturing process, does not change the sensitivity to parallel and perpendicular impacts.

4.2 Microfractographic Approach to the Load History Reconstruction

(Dorota Kocańda – Military University of Technology)

The problem of load history reconstruction for a failed component or structure on the basis of microfractographic analysis has been considered for many years. In the literature one can find both positive and negative opinions on the fractography capabilities within this scope.

Within the research presented the influence of variable amplitude load on the fatigue life of a 3 mm thick 2024-T3 aluminium alloy sheet was studied. The correlation was investigated as well between the images of fracture surface and the applied loads. Two variable amplitude load sequences were used in the fatigue tests; i.e., the LHL (low-high-low) block program (Fig. 4.2.1a) and the Flight-by-Flight cycle sequence (Fig. 4.2.1b),. These loads simulated the in-flight loads of the aircraft wing lower skin. Ten Flight-by-Flight sequences (each one of 240 cycles) correspond to one LHL program of 2400 cycles.

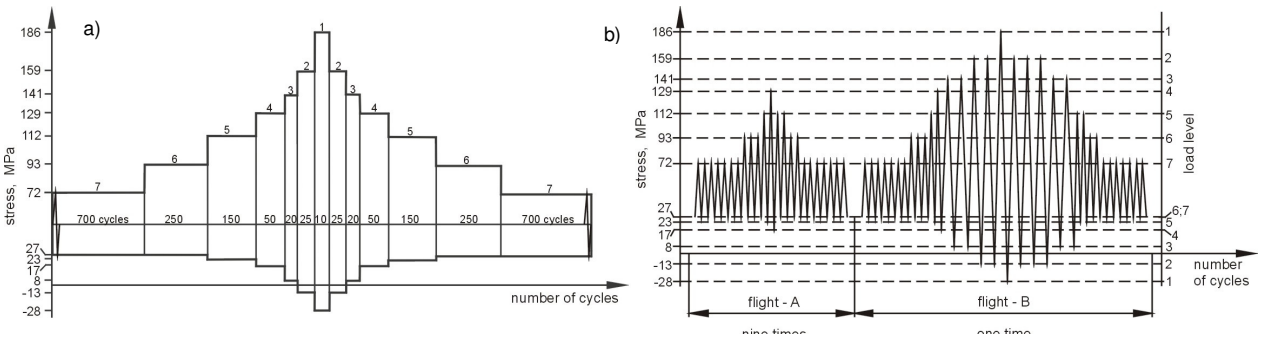

Figure 4.2.1. Schemes of LHL-100 block program (a) and Flight-by-Flight cycle sequence (b).

To investigate the load sequence effect on the fatigue crack growth the microfracture images obtained using a TEM microscope were analyzed. Sample results of TEM micrographs and diagrams of local crack growth rate versus the crack length for each examined load sequence are shown Fig. 4.2.2 and Fig.4.2.3

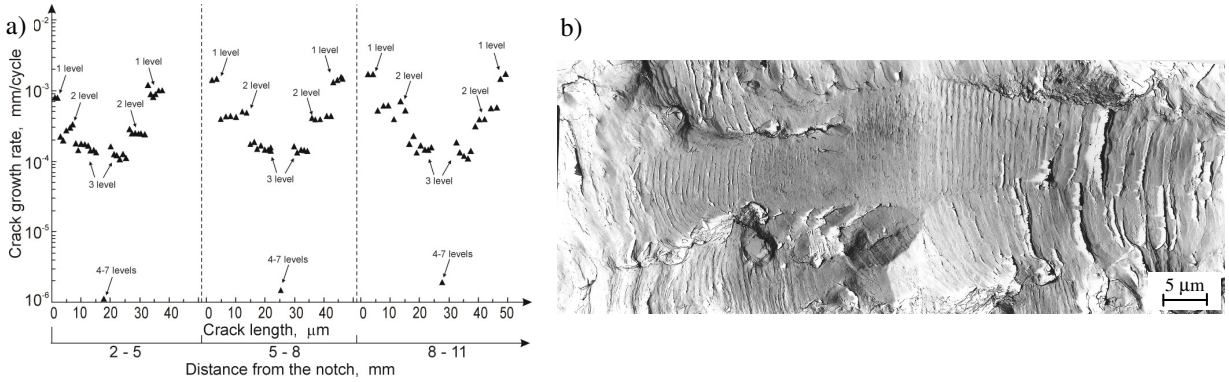

Fig. 4.2.2. Local crack growth rates versus crack length for three distances from the notch root (a) and TEM micrograph with the fatigue striation distributions (b) during the LHL load program.

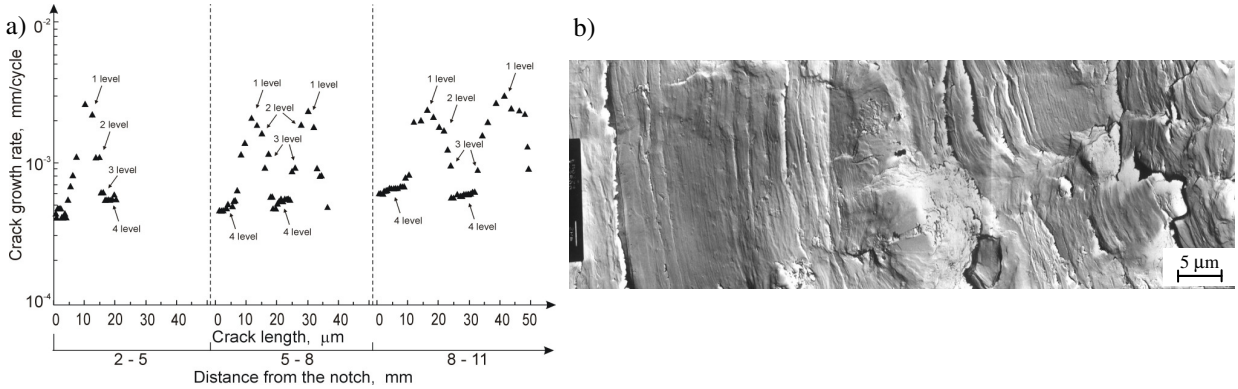

Fig. 4.2.3. Local crack growth rates versus the crack length for three distances from the notch root (a) and TEM micrograph with fatigue striation distributions (b) during the Flight-by-Flight load program

The results obtained show that it was possible to determine the correlation between the striation distributions and the applied group of cycles only for some special stress levels; namely from 1 to 3 levels in the case of LHL program and for 1 to 4 stress levels in the second loading program. That limited capability of load history reconstruction based on the microfracture analysis results from the crack closure caused by multiple overloads appearing cycle by cycle in the applied load programs.
The microfracture analysis proved that the period of crack propagation covered only 4.2 % of whole time of load application in the case of LHL program and 8.4% in the second load program, respectively. It means that for most part of the load application the crack growth was stopped or continued at very small rates. For this reason the fatigue striations were invisible on the fracture surface.

4.3 Fatigue Crack Growth in the Aluminium Alloy D16Cz

(Małgorzata Skorupa – University of Mining and Metallurgy)

Comprehensive fatigue crack growth investigations have been carried out on sheet specimens of the Russian aluminium alloy D16CzATWH which is similar to the American alloy 2124 and is commonly used in East Europe aviation industry. One of the reasons of test program carrying out was comparison between the test results and the data of 2024-T3 alloy which is equivalent to D16Cz alloy in view of application and mechanical properties and for which extensive crack growth data are available.

Investigations included constant amplitude (CA), variable amplitude (VA) and random loading fatigue tests and fatigue crack growth prediction by means of the strip yield model from the NASGRO software. The investigations were carried out in co-operation with professor Schijve of Technical University in Delft, Holland.
The CA tests were carried out to provide basic crack growth data for a comparison with the results of the VA tests and for predictions of the crack growth behaviour under VA loading. The VA test program included a fatigue test with a single overload (OL), tests with periodic overloads (OLs) and underloads (ULs) and flight-simulation tests employing the standardized load history miniFALSTAFF. The crack length was measured by a traveling microscope with an accuracy of ±0.01 mm for both crack tips and an average value of the two cracks was used in the evaluation of the results. Fractographic observations were made on all specimens and compared to the crack growth records.
The fatigue tests under the CA loading and with different stress ratios indicated similar crack growth results as those obtained for 2024-T3 Alclad reported in the literature. Also the miniFALSTAFF crack growth data were in good agreement with the results of test program on 2024-T3 sheet specimen reported in the literature.
The predictions of fatigue crack growth in D16Cz and 2024-T3 aluminium alloys were made performed with the use of the strip-yield model from the NASGRO software. The predictions were made for CA loading as well as for programmed and random VA load histories. The computations included either of the two different strip-yield model implementations available in NASGRO; i.e., constant constraint-loss (CCL) and variable constraint-loss (VCL) model and two types of the input material description (NASGRO equation and discrete da/dN vs. ΔK_{eff} data). The model performance was evaluated basing on comparisons between the predicted and observed results, respectively. The computed results were found to be strongly dependent on the combination of the material input data type and the constraint factor concept. Though all trends observed were qualitatively reflected in the strip-yield model predictions, the quantitative correlation between the computed and test results for the VA loading sequences is unsatisfactory and in some cases worse then that reported in the literature for a more simple semi-empirical crack closer model.

5. JOINTS

5.1 A Method for Analysis of Local and Micro-Local Physical Phenomena in Riveted Joints of a Thin-Walled Aircraft Structure

(Elżbieta Szymczyk – Military University of Technology)

The riveted joints are critical areas of the aircraft structure due to severe stress concentrations, plastic strain and the effects like surface wear (Fig. 5.1.1) and secondary bending. The fatigue crack initiation starts usually at the rivet holes, reducing therefore, the fatigue life of the riveted joint. The aim of the project consists in the analysis of local phenomena arising in the rivet–hole interface. The effect of fretting (frictional corrosion) has been chosen as one of the most interesting phenomena that emerge in the vicinity of a rivet and accelerate the fatigue processes.

Fig. 5.1.1. Fretting wear at the rivet hole.

The investigations were conducted in terms of the FEM analysis and modelling of the aircraft riveted joints as well as experiments made on specimens of riveted joints of a special design (Fig. 5.1.2), in which the fretting wear occurred. Within the framework of the project, static and fatigue tests were made for a riveted specimen consisting of aluminium alloy (D16 grade) sheets jointed with steel (St3 grade) rivets.

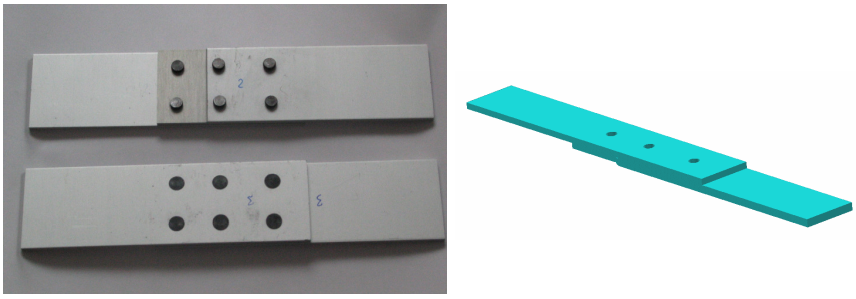

Fig. 5.1.2. Riveted specimen.

During the experiment the specimens were investigated by a non-destructive testing method (like brittle coatings, liquid penetrant inspection and visual detection analysis with a UV lamp (Fig. 5.1.3) to identify the technological and fatigue cracks and detect the surface wear. The X-ray diffraction method was used to determine residual stresses after the riveting process. The Optical and Scanning Electron Microscopes were employed for metallographic and fractografic analysis of the mating surfaces after the fatigue test.
The fatigue life of the specimen was equal to approximately 240000 cycles, while the fatigue life of specimens jointed with aluminium rivets was about two times higher on the logarithmic scale.

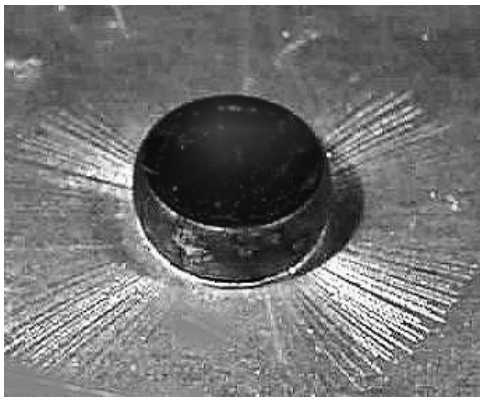

Fig. 5.1.3. Visual detections analysis.

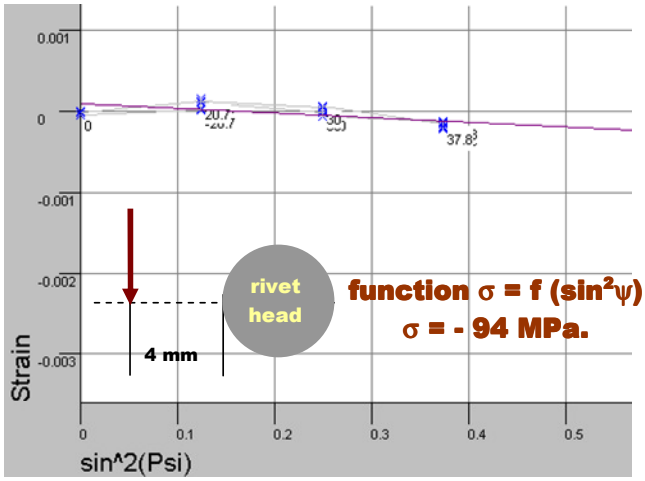

Fig. 5.1.4. X-ray diffraction measurement.

The comparative analysis of various non-destructive methods was conducted and their utility in estimation of the stress state in riveted joints was determined (Fig. 5.1.5). The brittle coating method was employed for the analysis of riveted joints. The applicability of effective and inexpensive visual methods to diagnostics of riveted joints has also been emphasized.

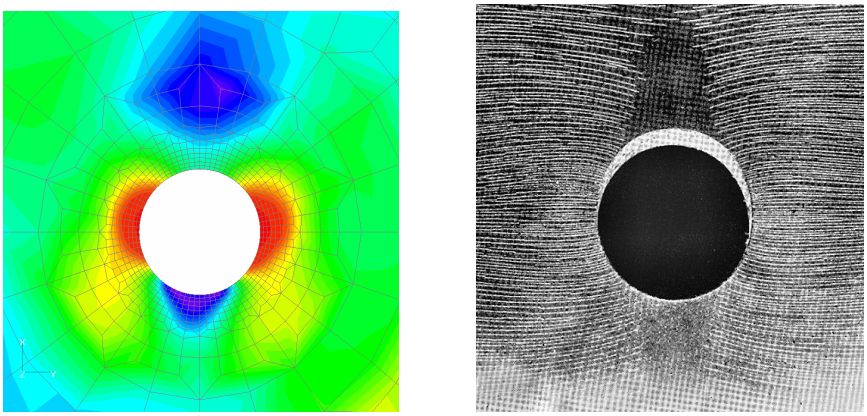

Fig. 5.1.5. Stress state around the rivet hole a) calculations b) experiment.

The influence of secondary bending in the tensile loaded lap riveted joint was taken into consideration. Surface, beam–surface, axisymetric and three–dimensional models, respectively, were analysed with the global, local and global–local analyses carried out to

verify the efficiency of each approach. The influence of numerical model parameters (like mesh density, shape of finite element in contact area) on the correctness of numerical simulation results was investigated. The influence of friction and material model on residual and service stress fields was studied. The relative displacements between a rivet and hole and the contact stress fields on the mating surface were calculated. A numerical representation of fretting having the form of a map of the work of friction forces has been put forward.
Numerical calculations and models were verified on the base of experimental tests (Fig. 5.1.6). The advantage of numerical simulation consists in lowering costs and improving the quality of analysis since more complete information can be provided about the stress and strain fields as compared to a pure experimental way.

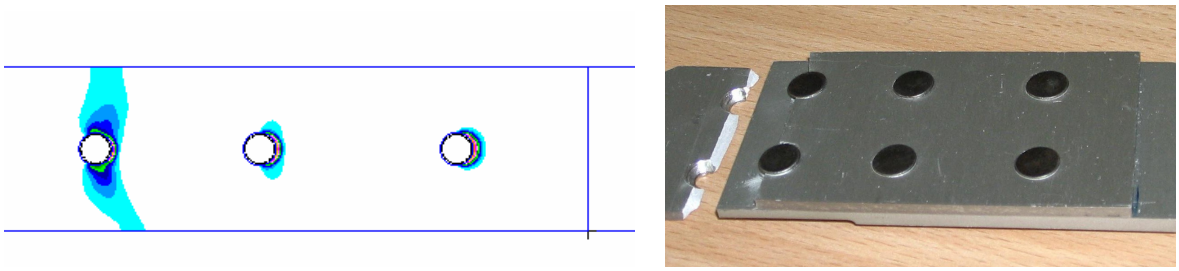

Fig. 5.1.6. Specimen after tensile loading.

The analyses conducted provide a more comprehensive knowledge of the contact problem and effects brought about by friction and crack initiation (microslips, fretting wear) in the riveted joints. The calculations made within the framework of the project allow one to determine the stress and strain intensity factors in the elasto-plastic range.
A wide range of studied and experimentally verified numerical models of the riveted joints justifies applicability of the presented methodology of modelling to further analysis, taking into consideration technological imperfections like gaps between a rivet and a hole and non-axial loading.
The knowledge of stress and strain states (Fig. 5.1.7), distributions of contact forces and relative displacements in the riveted joints, as well as corresponding images obtained by a visual detection methods allows for finding dangerous locations and crucial parameters (i.e. accuracy of manufacturing, risky cracks) in the aircraft structure, which should be under special control.

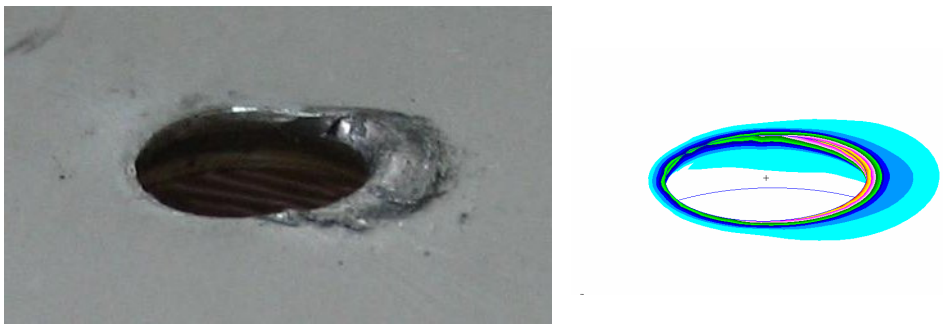

Fig. 5.1.7. Plastic strain field around the rivet hole.

A wide range of the considered visual methods for stress state determination in riveted joints allows for finding a proper diagnostic method suitable for both the service conditions and type of failure.
The research was conducted with the financial support of State Committee for Scientific Research(KBN) and has been continued within the EUREKA project IMPERJA.

5.2 Improving the Fatigue Performance of Riveted Joints in Airframes (IMPERJA)

(Jerzy Kaniowski – Institute of Aviation)

The project aims at increasing of the fatigue life of riveted joints, that can affect prolongation of the aircraft service life, reduce the number of inspections and lower the operation costs of an aircraft, respectively. The research team intends to achieve this goal by investigating and improving the riveting process as well as improving the prediction methods for the fatigue life.
Riveting is the method most commonly used for joining sheet metal components of the aircraft structure. Typically, the number of rivets ranges from several thousands to some millions in a single aircraft depending on the specific aircraft type and size. The riveted joints are critical areas of the aircraft structure due to severe stress concentrations and the effects; like, as fretting and secondary bending. Therefore, the fatigue crack usually initiates in the rivet hole region, sometimes even at a number of rivet holes (multiple site fatigue), which may cause a widespread fatigue damage and reduce the residual strength.
Although the literature on the fatigue behaviour of riveted joints is quite abundant, many aspects are still insufficiently understood and investigated needing therefore, additional study. Within the scope of the project the following consecutive steps have been proposed:

Stage I – Residual stress fields generated in the sheet by the riveting process for various types of rivets and riveting techniques will be investigated. On this basis, a combination of the rivet shape and riveting process conditions should be selected, so that an optimum residual stress field for a given joint type could be obtained. At the same time, a numerical analysis and modelling of the riveting process will be performed.

Stage II – Comprehensive experimental and numerical investigations will be performed to explore the effect of various features of riveted joints on the crack initiation and crack propagation behaviour. Specifically, the influence of residual stresses, secondary bending and load transmission by frictional forces in the joint will be considered. Also, a stress intensity factor solution that accounts for the above mentioned effects will be developed using the Finite Element Method (FEM) analyses.

Stage III – Basing on the results obtained at stages I and II, the design of selected riveted structural details of an operating airplane will be evaluated and its modification to improve the fatigue performance will be proposed. Also, a methodology for estimating of the fatigue life of an aircraft structure will be developed based on the FEM modelling of the structure at three different levels of complexity, i.e., complete structure, structural detail and single riveted joint, respectively, were considered.

6. OTHER RELEVANT WORKS

6.1 Limit Curves of Complex Stress-State Fatigue Strength in View of a New Hypothesis

(Daniel K. Dębski, Krzysztof M. Gołoś – Warsaw University of Technology,
Marek A. Dębski – Institute of Aviation)

One of the fundamental problems studied in the field of the fatigue strength consists in the determination of limit curves corresponding to a given complex stress-state. On the score of the fact that initiation of a fatigue damage usually takes place on the surface of element or specimen, as well as thin-walled structures, therefore, in fact we deal with the problem of plane stress-state (PSS).

According to the Huber-Mises hypothesis:

$$\sigma_r = \sqrt{\left(\sigma^2 + 3\tau^2\right)} \tag{1}$$

By dividing both sides of the above equation by Z_{go} we obtain:

$$\frac{\sigma_r}{Z_{go}} = \sqrt{\left(\left(\frac{\sigma}{Z_{go}}\right)^2 + 3\left(\frac{\tau}{Z_{go}}\right)^2\right)} \tag{2}$$

And assuming in agreement with the hypothesis that $Z_{go} / Z_{so} = \sqrt{3}$ and $\sigma_r = Z_{go}$ we find the formula for the limit curve:

$$1 = \left(\frac{\sigma}{Z_{go}}\right)^2 + \left(\frac{\tau}{Z_{so}}\right)^2 \tag{3}$$

Investigations, which have been carried out so far, revealed that equation (3) does not fit well to the fatigue experimental results recorded especially for the elements and specimens with notches. Gough [3, 4] presented the limit curve represented by the equation:

$$\left(\frac{\sigma}{Z_{go}}\right)^2\left(\left(\frac{Z_{go}}{Z_{so}}\right)-1\right) + \left(\frac{\sigma}{Z_{go}}\right)\left(2-\left(\frac{Z_{go}}{Z_{so}}\right)\right) + \left(\frac{\tau}{Z_{so}}\right)^2 = 1 \tag{4}$$

By putting down that $Z_{go} / Z_{so} = 2$ we obtain the limit curve equation in accordance with equation (3) that ensues from the Huber-Mises hypothesis, but unfortunately the hypothesis claims that $Z_{go} / Z_{so} = \sqrt{3}$.

In works [1, 2] another hypothesis was proposed, i.e. the one being in contradistinction to the classical Huber-Mises, $\sigma_{\max}$ or as much as $\tau_{\max}$ hypotheses. That one assumes fatigue damage initiation is tightly related to the existence of a notch that can emerge due to material non-homogeneity or is design-affected in a given load-carrying structure. A circular hole has been assumed to embody such a notch.
The hypothesis (in PSS) can be formulated as follows:

$$\sigma_r = \frac{\sigma}{3} + \frac{2}{3}\sqrt{\left(\sigma^2 + 4\tau^2\right)} \tag{5}$$

what yields the expected result $Z_{go} / Z_{so} = 4/3$; i.e., close to that obtainable for a steel shaft with a cross-bored hole for which (see [4], p. 975) the experimental result of that ratio was 1.38.

Similarly, as in the above, we obtain the limit curve equation:

$$1 = \frac{2}{3}\left(\frac{\sigma}{Z_{go}}\right) + \frac{1}{3}\left(\frac{\sigma}{Z_{go}}\right)^2 + \left(\frac{\tau}{Z_{so}}\right)^2 \qquad (6)$$

It can be seen that for $Z_{go} / Z_{so} = 4/3$ equations (4) and (6) become identical, and for $Z_{go} / Z_{so} = 2$ equation (4) becomes compatible with the limit curve equation (Eq. 3) according to the Huber-Mises hypothesis. Basing on the data available from the literature one can conclude that most of the experimental results is placed in between limit curves (3) and (6), see Fig. 6.1.1. For elements and specimens with notches the limit curve represented by Eq (6) is more appropriate according to the hypothesis presented in [1].

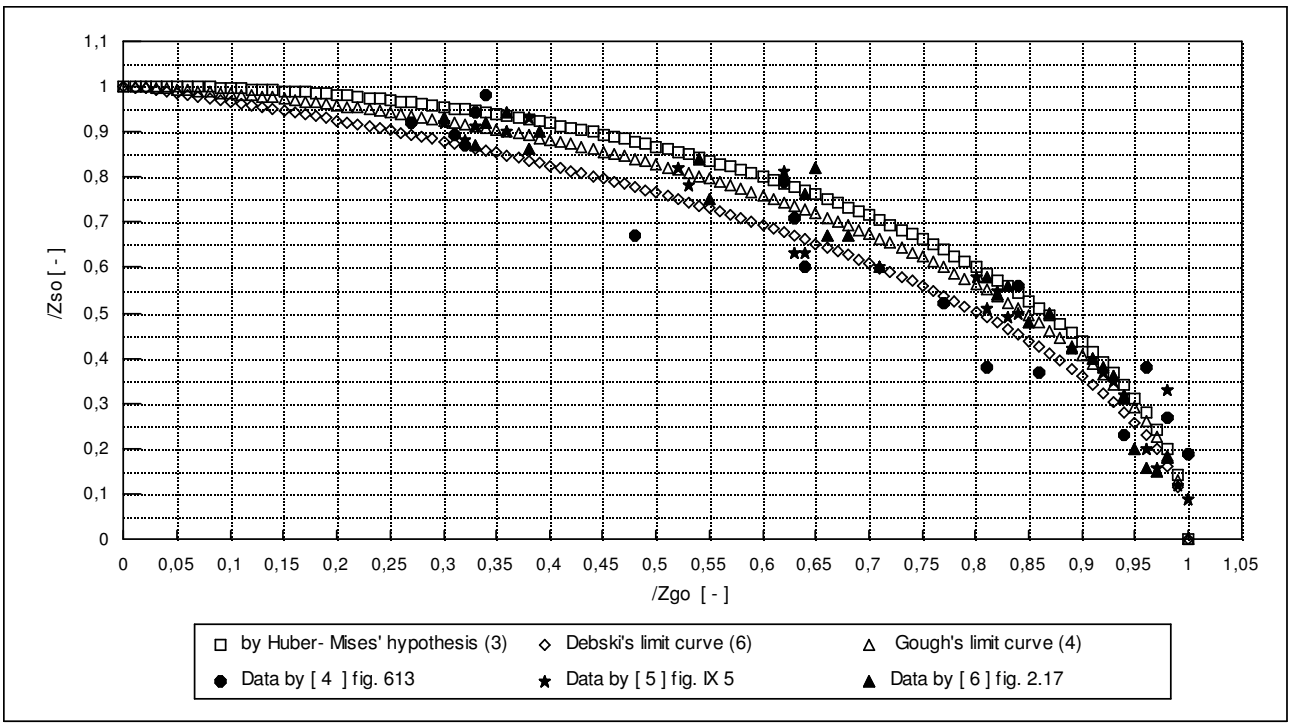

Fig. 6.1.1 Limit curves in complex stress-state.

If for $Z_{go} / Z_{so} = 2$, not as in the Huber-Mises hypothesis for $Z_{go} / Z_{so} = \sqrt{3}$, the Gough curve (Eq 4) assumes the shape of curve (3) and for $Z_{go} / Z_{so} = 4/3$ the shape of curve (6), then the coefficients of the Gough curve should be corrected. When equation (4) is written in the form:

$$\left(\frac{\sigma}{Z_{go}}\right)^2 A + \left(\frac{\sigma}{Z_{go}}\right) B + \left(\frac{\tau}{Z_{so}}\right)^2 = 1 \qquad (7)$$

then for $Z_{go} / Z_{so} = 2$ the coefficients are $A = 1$ and $B = 0$, and for $Z_{go} / Z_{so} = 4/3$ they become $A = 1/3$ and $B = 2/3$. In order to obtain the coefficient values: $A = 1$ and $B = 0$ for $Z_{go} / Z_{so} = \sqrt{3}$ – as it results from the Huber-Mises hypothesis – and assuming linear relationship within the range:

$$\frac{4}{3} \le \frac{Z_{go}}{Z_{so}} \le \sqrt{3}$$

we arrive

$$A = \frac{2}{3\sqrt{3}-4}\left(\frac{Z_{go}}{Z_{so}}\right) + \frac{\sqrt{3}-4}{3\sqrt{3}-4} \qquad (8)$$

$$B = \frac{-2}{3\sqrt{3}-4}\left(\frac{Z_{go}}{Z_{so}}\right) + \frac{2\sqrt{3}}{3\sqrt{3}-4}$$

With the accuracy sufficient enough we have:

$$A = 1.67\left(\frac{Z_{go}}{Z_{so}}\right) - 1.90$$

$$B = -1.67\left(\frac{Z_{go}}{Z_{so}}\right) + 2.90$$

while the limit curve assumes the form:

$$\left(\frac{\sigma}{Z_{so}}\right)^2\left(1.67\left(\frac{Z_{go}}{Z_{so}}\right) - 1.90\right) + \frac{\sigma}{Z_{so}}\left(-1.67\left(\frac{Z_{go}}{Z_{so}}\right) + 2.90\right) + \left(\frac{\tau}{Z_{so}}\right)^2 = 1 \qquad (9)$$

For which we obtain the limit curve according to the Huber-Mises hypothesis if $Z_{go} / Z_{so} = \sqrt{3}$, and the one corresponding to hypothesis (5) when $Z_{go} / Z_{so} = 4/3$.

Introduction of the strength hypothesis (Eq 3), that takes into account the existence on non-homogeneity of both the material and structure and reflects it in the form of the equivalent notch, has enabled determination of new limit curve corresponding to fatigue strength in a complex stress- state. This has also enabled correction of the Gough limit curve, making it for given Z_{go} / Z_{so} ratios fully consistent with the limit curves derived from the Huber-Mises as well as (3) hypotheses.

References

[1] *Dębski M.*: Hypothesis of maximum stress at the edge of the circular hole notch, Aeronautics and Astronautics Engineering, No 6, 1987.
[2] *Dębski M.*: The effort hypothesis in fatigue calculations of riveted aircraft structures, Transactions of the Institute of Aviation, No137, 1994
[3] *Gough H. J.*: J. Appl. Mech. 17(1950)
[4] *Nemec. J.*: Strength and stiffness of steel elements, W. N. - T. Warszawa 1968
[5] *Buch A.:* Problems of the fatigue strength, PWN 1963
[6] *Kogajew B. П.*: Durability calculus for time-variable stress-state, Moskwa „Mashinostrojenie" 1977.

6.2 Continuous Fatigue Estimation of Airplane Structures

(Marek Dębski – Institute of Aviation)

The research was focused on implementation of the idea of continuous estimation of fatigue and safety level of aero structures and other structures using load and fatigue recorders.
The proposed approach allows for:

- improving the exploitation safety,
- service life extension,
- evaluation of the real fatigue and exploitation intensity in each construction,
- putting recorders at any chosen points on the structure – even those of difficult access,
- acquisition of statistical data for verification and development of the load spectrum for aircraft, ships and other structures.

Aircraft Autonomous Loads Recorder – AROS

The progress in electronics allowed us to design the autonomous recorder- ***Aircraft Autonomous Fatigue Loads Recorder AROS***. (Mass: 0.25 kg).
The built-in accelerometer is the source of the signal.
The cell allows recorder to work continuously for two years. Software of the recorder registers the signal, analyzes and shows the results.
The test program of the recorder is being conducted in laboratories of the Institute of Aviation in order to obtain the certificate.
The first flight test was conducted using the small aerobatic radio plane RC Feniks.
Now, Aros is being tested in flight on the following aircraft: I-23 Manager, M-18 Dromader and TS-11 Iskra.

Autonomous Fatigue Recorder – AFR

Autonomous Fatigue Recorder - AFR is a kind of small computer. The processor Texas Instruments MSP–430 is the main part of the recorder. Software of AFR for signal analysis was written in C and Assembler programming languages.
There are two kinds of sources of the signals in AFR:

- built-in accelerometer,
- external sensors placed in the critical points of the structures.

At the first stage of measurement the AFR software registers and analyzes the fatigue load spectrums at the critical points of structures.
For the signal classification (analysis) the following methods were used:

• classic method of the cycles reductions, used for estimation of the aircraft fatigue load spectrum,
• full cycles method – 3D diagram
It is also possible to apply any method required by the user.
Following that the software provides us with the estimation of current fatigue consumption

level of the structure, which is defined by the following coefficients:

• **FF** - Fatigue Factor (fatigue due to the real exploitation loads)
• **FIF** - Fatigue Intensity Factor
• **ETF** - Exploitation Time Factor
FF = ETF * FIF
The data used in calculations were as follows:
- Fatigue characteristics (the Wholer characteristics) of the structures or of the critical points of the structures, or results of the fatigue tests
- Fatigue load spectrum (from the previous stage)

The AFR recorder became the main element of the Idea of the Continuous Estimation of Fatigue of Structures.
As a result of the AFR recorders application one attains:
• optimal exploitation
• safety control of the structures
If you need some more information please, visit the web sites:
Institute of Aviation: http://www.ilot.edu.pl/STRANG/index.htm
AROS: http://www.ilot.edu.pl/STRANG/Designs/aros.htm
AFR: http://www.ilot.edu.pl/STRANG/Designs/AFR.pdf
AFR: http://www.aerosme.com/asp/pps1.asp#